PPPL Calculation Form - No: NSTXU-CALC-55-04

Calculation # NSTXU-CALC-55-04 Revision # 0 ____ WP #, if any (ENG-032) 2254 ____

Purpose of Calculation: (Define why the calculation is being performed.)

The purpose of this calculation is to validate coil terminal stresses at lead sections of the inner PFs with the new design of filler blocks, support brackets and bus bar structure assembly for all six PF1 coils.

Codes and versions: (List all codes, if any, used)

ANSYS 18.2

References (List any source of design information including computer program titles and revision levels.)

[1] NSTX-U-RQMT-GRD-001-00 General Requirements Document, S. Gerhardt, December, 2017

[2] NSTX-U-RQMT-SRD-002-00 System Requirements Document Magnet Systems, S. Gerhardt, December, 2017.

[3] Inner PF coil design parameters, M. Kalish, February, 2018.

[4] NSTX-CRIT-0001-02 Structural Design Criteria, I. Zatz, January, 2016

[5] NSTX-U-SPEC-MAG-001-2 Specification for Inner PF coil conductor, M. Kalish, November, 2017

[6] MAG-171221-YZ-02, PF1A conductor dimension and cooling hole size, NSTX-U engineering memo, Y. Zhai, December, 2017.

[7] NSTX-U_RQMT-RD-012-00, Inner-PF Coil Interfaces to Supports Designs and Cooling Systems, S. Gerhardt, March, 2018.

[8] MAG-180306-YZ-01, Material Properties for Inner PF Coil FDR, MAG-180306-YZ-01, March, 2018.

[9] NSTX-U-CALC-133-09-00, OH Conductor Fatigue and Fracture Mechanics Analyses, Titus, November, 2010.

[10] NSTX-U-CALC-133-24, Calculation of Inner PF Coil Fatigue and Fracture Mechanics, Y. Zhai, March, 2018.

[11] NSTX-U-CALC-133-28, Summary of Loads for Inner PF Leads and Bus Bars Analysis, Y. Zhai, March 20, 2018.

[12] NSTX-U-CALC-131-27, Inner PF Coil Thermal Analysis, Y. Zhai, March 14, 2018.

[13] NSTX-CALC-11-01-00, Global Thermal Analysis of Center Stack Heat Balance, A. Brooks, February 15, 2011.

[14] NSTXU-CALC-55-08-00 PF1cL Terminal Lead and Bus Bar, AKhodak, Checked by W.Wang

[15] NSTXU-CALC-55-06-00 PF1cU Terminal Lead and Bus Bar, Wenping Wang Checked by A. Khodak

[16] Inner PF Drawing Series e-dc11101_32718, e-dc 11102-03271 (PF1a) , e-dc 11100_32718

[17] NSTXU-CALC-133-24-00 Fatigue Analysis and Crack Growth, Yuhu Zhai

[18] NSTXU-CALC-133-27-00 Generation of PF Bus Load Files, Yuhu Zhai

Assumptions (Identify all assumptions made as part of this calculation.)

The 3D structural analysis models with conductor spiral winding, coil terminals and new bus bar assembly for each of the PF-1a, 1b and 1c coil are developed and used for the lead analysis. For the upper inner PF-1a and PF-1b, the worst CS vertical displacement of 5 mm relative to the vacuum vessel is used. The end of pulse condition is used where the maximum coil temperature of 60 C, 90 C and 50 C for the PF-1a, OF-1b and PF-1c coils are prescribed in the lead analysis. The body force density cloud data extracted from the 3D MAXWELL magnetostatic analysis for the worst case EQ scenarios of $51, #33 and #18 for PF-1a, PF-1b and PF-1c coils are mapped onto the spiral wound conductors, coil terminals and the bus bars in the structural analysis models. The pre-load mechanism were considered in the 3D lead analysis of PF-1a and PF-1b coils via a number of springs (set screws) on the pressure plate of the coil sling support structures. Linear structural analyses are performed for each inner PF coil where spiral winding of conductors is modeled but smeared properties are assumed as coil pack insulations. This report is to summarize the stress results from 3D calculation of coil terminal lead sections for the new design of the inner PFs.

Calculation (Calculation is either documented here or attached)

Please see attached main body of this document.

Conclusion (Specify whether or not the purpose of the calculation was accomplished.)

Magnetostatic analysis and 3D static structural analyses were performed for the inner PF coils PF-1a, -1b and -1c 3D models including conductor spiral winding, terminals and bus bars. The structural analysis for all six coil terminals follows consistently a procedure developed for 3D lead analysis. The main conclusions include

1. *The design of terminal support filler blocks, support brackets as well as clamping of the two bus bars to be more effective in reacting Lorentz forces is critically important to ensure the peak stress on the conductors in the lead sections can be minimized.*

2. *Although coil terminals will experience large Lorentz forces, with the optimized support structure, peak stress under EM load only on coil terminals is well within the fatigue design limit. The stress under the thermal loads due to temperature gradient at the terminal region, however, can contribute more appreciably.*

3. *The local peak stress on the inner PF coils for all inner PFs is within the 160 MPa fatigue design allowable.*

Additional design features such as .25" radius fillets to all the coil terminal flags are implemented into the final inner PF1 design so to mitigate risk associated with the geometry discontinuity at the conductor and terminal flag interfaces.

Preload mechanism is implemented in the 3D analysis models (PF-1a and PF-1b Lower) via the springs (with an adjustable stiffness) to capture motion of the coil pack under various different local cases.

Cognizant Individual (or designee) printed name, signature, and date Steve Raftopoulos Digitally signed by Steve Raftopoulos Date: 2018.09.12 09:55:33 -04'00'

Preparer's printed name, signature and date

Yuhu Zhai Digitally signed by Yuhu Zhai Date: 2018.09.10 12:42:19 -04'00'

I have reviewed this calculation and, to my professional satisfaction, it is properly performed and correct.

Checker's printed name, signature, and date Peter H. Titus Digitally signed by Peter H. Titus Date: 2018.09.12 16:40:28 -04'00'

National Spherical Torus eXperiment - Upgrade

NSTX-U

Inner PF Coil Leads and Bus bars Analysis

NSTXU-CALC-55-04 - Rev 0

March 29, 2018

Yuhu Zhai Digitally signed by Yuhu Zhai Date: 2018.08.07 10:56:21 -04'00'

Yuhu Zhai_____________Thomas Willard

Prepared By

Peter H. Titus Digitally signed by Peter H. Titus Date: 2018.03.29 22:08:16 -04'00'

Art Brooks_______________ Peter Titus

Reviewed By

Michael Kalish Digitally signed by Michael Kalish Date: 2018.03.30 07:40:36 -04'00'

____________Mike Kalish_______________

Approved By – Responsible Engineer

Steve Raftopoulos Digitally signed by Steve Raftopoulos Date: 2018.03.30 10:12:05 -04'00'

NSTX-U CALCULATION

Record of Changes

Rev.	Date	Description of Changes	Revised by
0	3/20/18	Initial Release	Yuhu Zhai

NSTX-U ENG-33 Calculation Form

Purpose of Calculation:

The purpose of this calculation is to validate coil terminal stresses (at lead sections) of the inner PFs with the new design of filler blocks, support brackets and bus bar structure assembly for all six PF1 coils.

References:

[1] NSTX-U-RQMT-GRD-001-00 General Requirements Document, S. Gerhardt, December, 2017

[2] NSTX-U-RQMT-SRD-002-00 System Requirements Document Magnet Systems, S. Gerhardt, December, 2017.

[3] Inner PF coil design parameters, M. Kalish, February, 2018.

[4] NSTX-CRIT-0001-02 Structural Design Criteria, I. Zatz, January, 2016

[5] NSTX-U-SPEC-MAG-001-2 Specification for Inner PF coil conductor, M. Kalish, November, 2017

[6] MAG-171221-YZ-02, PF1A conductor dimension and cooling hole size, NSTX-U engineering memo, Y. Zhai, December, 2017.

[7] NSTX-U_RQMT-RD-012-00, Inner-PF Coil Interfaces to Supports Designs and Cooling Systems, S. Gerhardt, March, 2018.

[8] MAG-180306-YZ-01, Material Properties for Inner PF Coil FDR, MAG-180306-YZ-01, March, 2018.

[9] NSTX-U-CALC-133-09-00, OH Conductor Fatigue and Fracture Mechanics Analyses, Titus, November, 2010.

[10] NSTX-U-CALC-133-24, Calculation of Inner PF Coil Fatigue and Fracture Mechanics, Y. Zhai, March, 2018.

[11] NSTX-U-CALC-133-28, Summary of Loads for Inner PF Leads and Bus Bars Analysis, Y. Zhai, March 20, 2018.

[12] NSTX-U-CALC-131-27, Inner PF Coil Thermal Analysis, Y. Zhai, March 14, 2018.

[13] NSTX-CALC-11-01-00, Global Thermal Analysis of Center Stack Heat Balance, A. Brooks, February 15, 2011.

[14] NSTXU-CALC-55-08-00 PF1cL Terminal Lead and Bus Bar, AKhodak, Checked by W.Wang

[15] NSTXU-CALC-55-06-00 PF1cU Terminal Lead and Bus Bar, Wenping Wang Checked by A. Khodak

[16] Inner PF Drawing Series e-dc11101_32718, e-dc 11102-03271 (PF1a) , e-dc 11100_32718

[17] NSTXU-CALC-133-24-00 Fatigue Analysis and Crack Growth, Yuhu Zhai

[18] NSTXU-CALC-133-27-00 Generation of PF Bus Load Files, Yuhu Zhai

Assumptions:

The 3D structural analysis models with conductor spiral winding, coil terminals and new bus bar assembly for each of the PF-1a, 1b and 1c coil are developed and used for the lead analysis. For the upper inner PF-1a and PF-1b, the worst CS vertical displacement of 5 mm relative to the vacuum vessel is used. The end of pulse condition is used where the maximum coil temperature of 60 C, 90 C and 50 C for the PF-1a, PF-1b and PF-1c coils are prescribed in the lead analysis. The body force density cloud data extracted from the 3D MAXWELL magnetostatics analysis for the worst case EQ scenarios of #51, #33 and #18 for PF-1a, PF-1b and PF-1c coils are mapped onto the spiral wound conductors, coil terminals, and the bus bars in the structural analysis models. The pre-load mechanism were considered in the 3D lead analysis of PF-1a and PF-1b coils via a number of springs (set screws) on the pressure plate of the coil sling support structures. Linear structural analyses are performed for each inner PF coil where spiral winding of conductors is modeled but smeared properties are assumed as coil pack insulations. This report is to summarize the stress results from 3D calculation of coil terminal lead sections for the new design of the inner PFs.

Calculation:

Included in the body of the calculation

Conclusion:

Magnetostatic analysis and 3D static structural analyses were performed for the inner PF coils PF-1a, -1b and -1c 3D models including conductor spiral winding, terminals and bus bars. The structural analysis for all six coil terminals follows consistently a procedure developed for 3D lead analysis. The main conclusions include

1. *The design of terminal support filler blocks, support brackets as well as clamping of the two bus bars to be more effective in reacting Lorentz forces is critically important to ensure the peak stress on the conductors in the lead sections can be minimized.*

2. *Although coil terminals will experience large Lorentz forces, with the optimized support structure, peak stress under EM load only on coil terminals is well within the fatigue design limit. The stress under the thermal loads due to temperature gradient at the terminal region, however, can contribute more appreciably.*

3. *The local peak stress on the inner PF coils for all inner PFs is within the 160 MPa fatigue design allowable*.

Additional design features such as .25” radius fillets to all the coil terminal flags are implemented into the final inner PF1 design so to mitigate risk associated with the geometry discontinuity at the conductor and terminal flag interfaces.

Preload mechanism is implemented in the 3D analysis models (PF-1a and PF-1b Lower) via the springs (with an adjustable stiffness) to capture motion of the coil pack under various different local cases.

Contents

1. Executive Summary

The NSTX-U inner PF coils are water-cooled copper solenoids fabricated from rectangular or square shaped conductors with embedded central cooling channels. The coils, consist of three upper and lower pairs, denoted PF-1a, PF-1b and PF-1c, are energized up to 20 kA for about 1-2 seconds during plasma operations and then cooled down with 12 0C cold water once every 1200 seconds. Detailed drawings of the coils and their terminals are listed in [16] During machine operation the conductors in coil terminals (lead sections) will experience large Lorentz forces (30-50 kN/m) from 2-3 T toroidal magnetic fields as well as differential thermal stresses between coil leads and bus bars when coils are pulsed. This calculation is to validate coil terminal stresses (at lead sections) of the inner PFs with the new design of filler blocks, support brackets and bus bar structure assembly for all six PF1 coils.

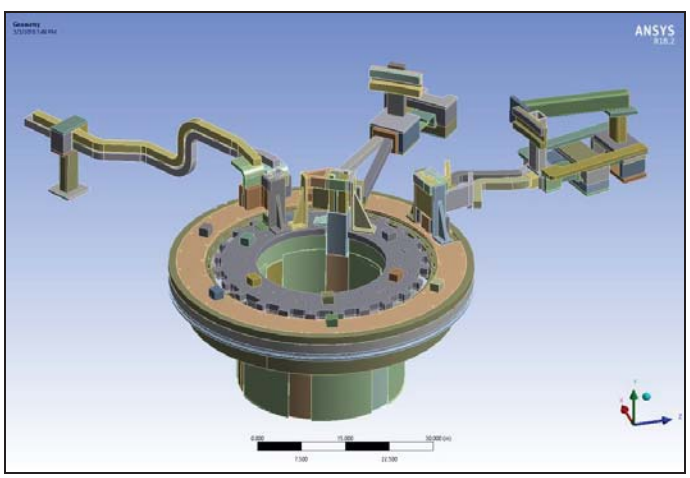

Figure 1.0-1 Upper PF Model - Note: PF1c (at Right) is included in Other Calculations [14], [15]

The fatigue stress allowable in the conductor when coils are pulsed shall be below 160 MPa fatigue stress limit. The PF1 Coils are heated up to the maximum temperatures almost instantaneously and uniformly when pulsed but Lorentz forces on coil leads and bus bars are maximized for the worst EQ scenarios when coils are running at ~20 kA full currents. The worst EQ scenarios for each coil are identified first and 3D magnetostatics analyses of the worst scenarios are performed using ANSYS MAXWELL 3D for each coil with detailed spiral winding and new bus flags and bus bar assembly. The body force densities on the coils, coil terminals and bus bars are mapped onto the 3D structural analysis models. Previous analyses indicated that the maximum lead stress is sensitive to the design of terminal filler blocks and support brackets, The new results from both positive and reverse toroidal fields under the worst case EQ scenarios show that a good structural design of support brackets at coil terminals to effectively react the Lorentz forces on coils and bus bars is the most important way to minimize peak stress on coil leads. With the new support brackets for coil leads and terminal flags, coil design meets the fatigue stress requirements per NSTX-U General Requirements Document [1] and the System Requirements Document for Magnet Systems [2]. The inner PF coils for NSTX-U are installed to provide the poloidal field shaping and better controlling of plasma in the diverter region during machine operations. The inner PFs, fabricated from rectangular or square shape copper conductors with embedded central cooling channels, are designed to have 20,000 pulse cycles over the lifetime of machine operation as defined in the latest General Requirement Document [4]. The key design requirements include 1) all coil designs shall allow for operation of the toroidal field in either direction, and of the plasma current in either direction, 2) static EM loads are defined in the Design Point Spreadsheet which disruption loads are derived from the NSTX-U disruption analysis requirements 3) the maximum temperature for operations shall be below 100 ^{0}C. To this end, 3D electromagnetic-structural coupled analyses were performed based on the worst EQ scenarios selected from the 2D axis-symmetric models of PF-1a, PF-1b and PF-1c maximum fields, Lorentz forces and coil stresses. The 2D results show that maximum temperatures on the conductor when pulsed are 58, 90 and 48 ^{0}C for PF-1a, -1b and -1c coils respectively and the maximum radial fields on the inner PFs are ~2 T from the worst case EQ scenarios for each inner PF coil. According to the NSTX-U structural design criteria [5], a fatigue strength evaluation is required for structural components including conductors and insulations, with undetectable flaws that are either cycled over 10,000 times during their operational lives or are exposed to cyclic peak stresses exceeding its yield stress. A fatigue strength evaluation is performed for the 2D coil winding pack. As an important part of the coil design validation process, the fatigue strength evaluation includes meeting requirements of either the design Stress-N (S-N) fatigue curve derived from material test data, or the crack growth limitation for the 20,000 cycles.

Table 1 – Summary of Peak Stress on Coil Leads from PF1 Upper

Fatigue	1A	1B
Stress Limit (MPa)	160	160
Peak Stress (MPa)	184 (Tresca) 150 (Max Principal)	150 (Tresca)

Table 2 – Summary of Peak Stress on Coil Leads from PF1 Lower

Fatigue	1A	1B
Stress Limit (MPa)	160	160
Peak Stress (MPa)	159	160 to 190 Tresca

Stresses that are compared with fracture mechanics derived allowables, should be max principal stresses. Or stresses perpendicular to a crack front Modeling of the flag to conductor includes a 90 degree intersection that is modeled in Workbench with bonded interface elements. To improve the stress concentration factor at this corner. And to move the peak stress away from the braze joint, The flags will be machined with .25 inch radius.

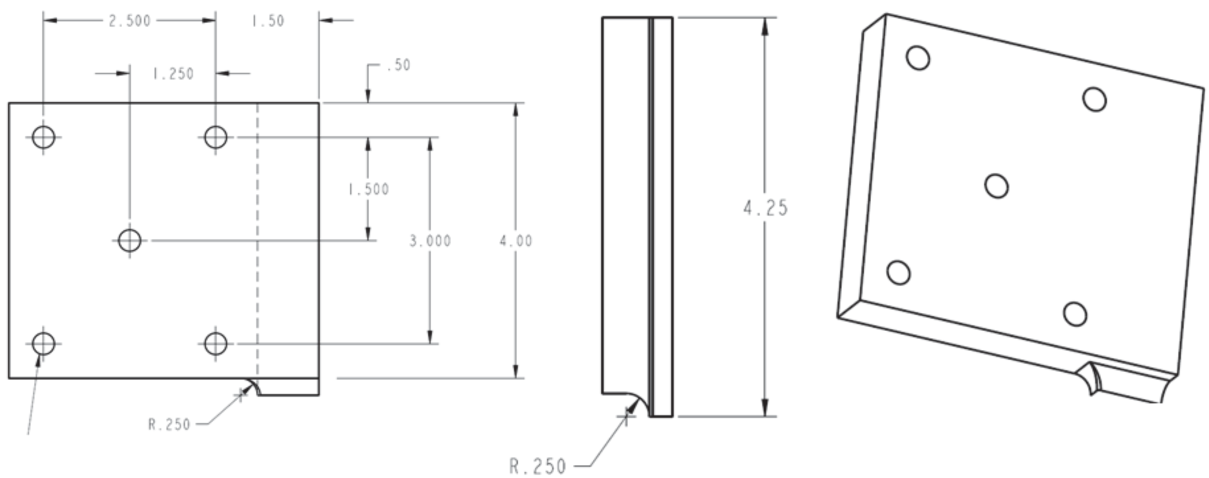

Figure 1.1-2 Flag Details from [16] for the 1a Coil

2. Inner PF Coil Design

Final drawings of the coils are listed in Reference [16]. The analysis was performed along with preparation of the drawings and includes pertinent details important for the stress evaluation. The coil geometry and conductor dimension of the global EM analysis models are taken from the latest Kalish Coil Design Parameter data sheet [3]. To ensure a self-consistent coil alignment with consideration of assembly and positional tolerances of components, the PF-1a conductor width was reduced by 1 mm since inner PF PDR so to increase the inner bore size by 8 mm (4 mm on each side), and cooling hole size is reduced from 0.225” to 0.185” accordingly so to maintain the same width from the hole edge to the conductor outer side edge for fatigue crack propagation of 1mm minimum detectable flaws. The Equivalent Square Wave (ESW) for PF-1a is reduced accordingly from 2.1s to 1.9s so to maintain the same maximum temperature with the conductor modification. The updated physics requirements for inner PFs are listed in Table 1.

Table 3 – Inner PF Physics Requirements

	PF-1a	PF-1b	PF-1c
No. of turns	61	20	16
Max current (kA)	19.67	20	20.25
ESW time (s)	1.9	1.0	1.4

Tables 2-3 listed the coil design parameters and the inner PF conductor dimensions [3], used as the input to establish the 2D axis-symmetric thermal analysis models. Figure 1 presents the analysis models for inner PF-1a and PF-1b upper and lower assembly in the polar region of NSTX-U. The structural models are used for the 3-D lead analysis.

Table 4 – Inner PF Coil Design Parameters

		MK PF Coil Sizing 02-01-18					
		PF1A (")	**PF1B** (")	**PF1C** (")	**PF1A** (mm)	**PF1B** (mm)	**PF1C**
R center	r_0=	**12.81**	15.44	21.85	325.374	392.176	554.99
Z center	z_0=	62.62	71.03	71.4	1590.548	1804.16	1813.56
Coil ID	ID=	**23.03**	29.32	41.66	585	745	1058
Coil OD	OD=	28.21	32.44	45.74	717	824	1162
Width	w=	**2.59**	1.56	2.04	58.1152	31.9532	44.1452
Height	h=	18.44	7.17	6.94	468.376	174.447	168.605

Table 5 – Inner PF Conductor Dimension

Conductor	PF1A (")	PF1B	PF1C	PF1A (mm)	PF1B	PF1C
Width	**0.481**	0.54	0.78	12.2174	13.716	19.812
Height	0.98	0.5	0.61	24.892	12.7	15.494
hole	**0.185**	0.146	0.146	4.699	3.7084	3.7084

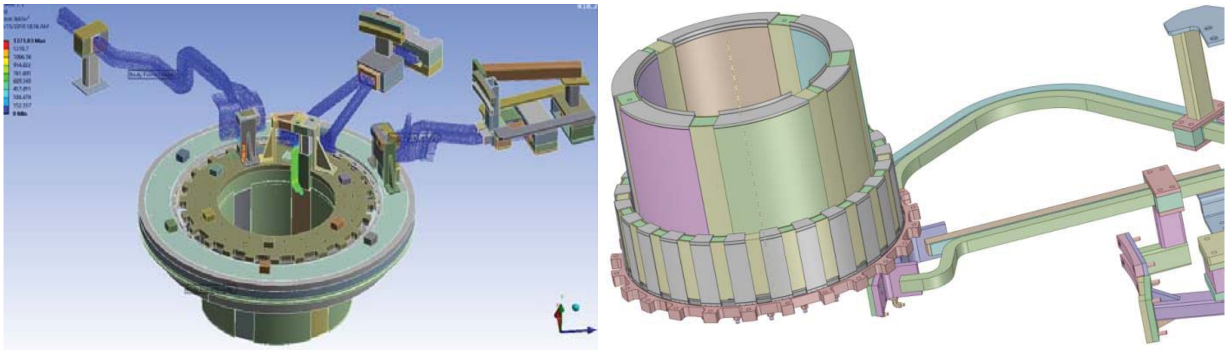

Figure 2.0-1 Structural Analysis Models for PF1a & 1b upper (top) and lower (bottom)

3. Structural Design Limits

According to [5], fatigue S-N fatigue curves shall be obtained based on the uniaxial strain cycling tests at service temperatures and at various R ratios. S-N fatigue curves shall be developed for both the base metal and for braze joints in the coil lead region.

a. The conductor static stress design limit is derived from the minimum yield strength given in the specifications for the inner PF conductors
b. The fatigue limit for copper is derived from the copper fatigue S-N curve

Figure 2 presents the copper conductor fatigue S-N curve from test data available from a number of references. For S-N fatigue evaluation, the more strict criteria of 2 on stress and 20 on life must be met. For the fracture mechanics evaluation, a factor of 2 on minimum detectable flaw size, 1.5 on fracture toughness, and 2 on life must be met. The measured NSTX OH conductor braze joint fatigue life is also included in the evaluation, along with the published S-N data for comparison. The conductor design limit for the OH coil design is 125 MPa [9]. The revised fatigue limit for the PF1 coil leads is summarized in the calculation [10] and shown in Figure 3.

A new procedure [11] has been developed for coil leads and bus bar analysis, which includes the following steps

- Setup structural environment in 3D models with coil spiral winding for the leads to be analyzed. Implement new design of the filler blocks at coil terminals, bus flags and bus bars.
- Import Lorentz forces from the worst case scenarios and maximum conductor temperatures on coil packs, leads and bus bars for static structural analysis
- Perform 3D EM and structural analysis for both positive and reverse toroidal field cases for the selected scenarios for each coils
- Check consistency throughout all lead analysis for each inner PFs

- *NSTX-U Structural Design Criteria*
  - Coils are evaluated by comparing Tresca stress to design limits
  - Main loads include EM (96 EQ) and Thermal during cool down

Stress Category	Parameters	Stress Intensity Limits
General primary membrane	P_m	$k\ S_m$
Local primary membrane	P_L	$1.5\ k\ S_m$
Primary membrane plus bending	$(P_m + P_b)$ or $(P_L + P_b)$:	$1.5\ k\ S_m$
Primary plus secondary	$(P_m + P_b + Q)$ or $(P_L + P_b + Q)$	$3\ S_m$

- *S_m - design stress limit, based on load cases*
  - *k*-factor – Normal operation *k = 1.0*
  - Anticipated events *k = 1.1*
  - Unlikely events: *k = 1.2*

Figure 3.0-1 Static Design Criteria

- *Static*
  - S_m is the smaller of $^2/_3\ \sigma_y$ or $^1/_2\ \sigma_u$ at the service temperature

σ_y (MPa)	σ_u	S_m	$1.5{*}S_m$	$3{*}S_m$	Temperature
103	221	69	103	207	20 C
93	198	62	93	186	100 C

- *Fatigue* - Total cycles of 20,000 – *NSTX CSU Pulse Spectrum*

Criteria	Stress Level ant Type	Actual
SN 2 on stress	112 MPa (Tresca)	142
SN 20 on life	180 (Tresca)	142
Fracture Mechanics with a flaw size less than .7mm 1.5 on KIc and 2 on Cycles	140 MPa (Max Principal or Hoop)	101
4 on cycles	125 MPa (Max Principal or Hoop)	101

Conductor Fatigue and Fracture Mechanics Analyses

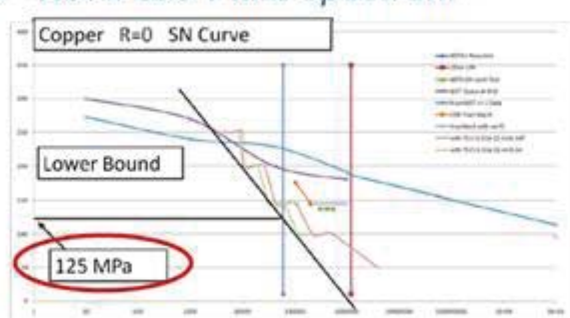

Figure 2 SN and Fracture Mechanics Fatigue Life

Figure 3.0-2 Structural Design Criteria and Conductor Static and Fatigue Limits

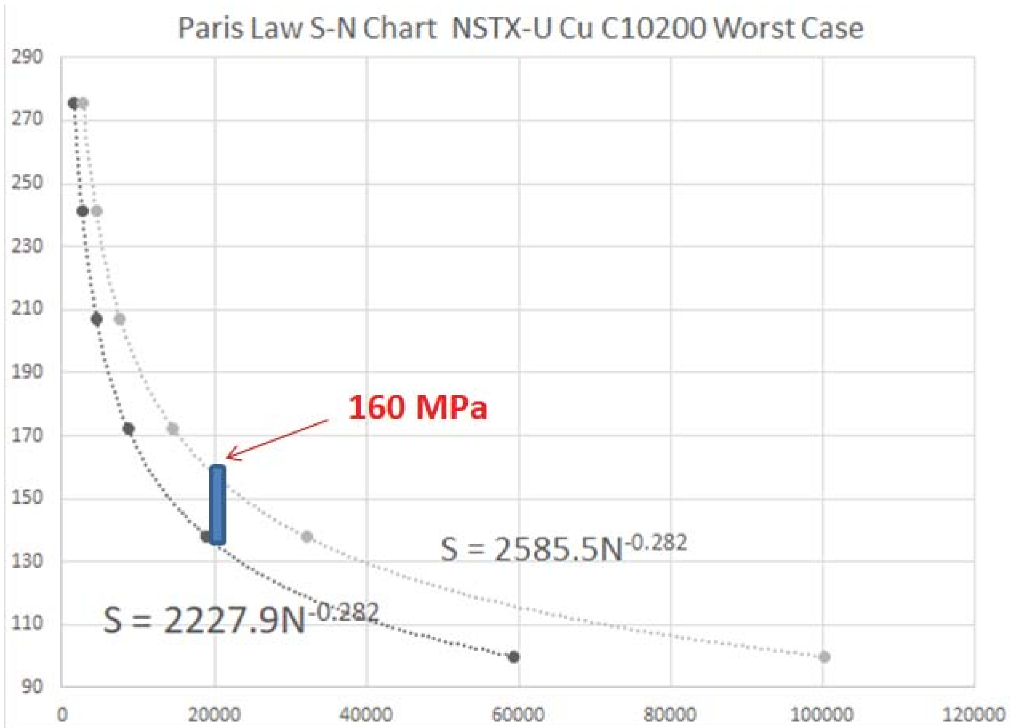

Figure 3.0-3 Revised Conductor Fatigue Crack Growth Limits – Stress vs. Cycles for PF1a conductor with Crack Growth Length of 2 mm (black) and 3.75 mm (gray). The modified 1a conductor maintained 3.75 mm crack growth path.[17]

4. Coil Lead and Bus bar Analysis

Three-dimensional magneto-static analysis models were developed for each of the upper and lower PF1-a, PF1-b and PF1-c coils as shown in Figure 4 below. The 3D EM models include conductor spiral winding, coil leads, bus flags and bus bar assembly. Figure 4 also showed the magnetic field distribution in the vertical plane, as well as the detailed coil spiral winding used for the lead analysis.

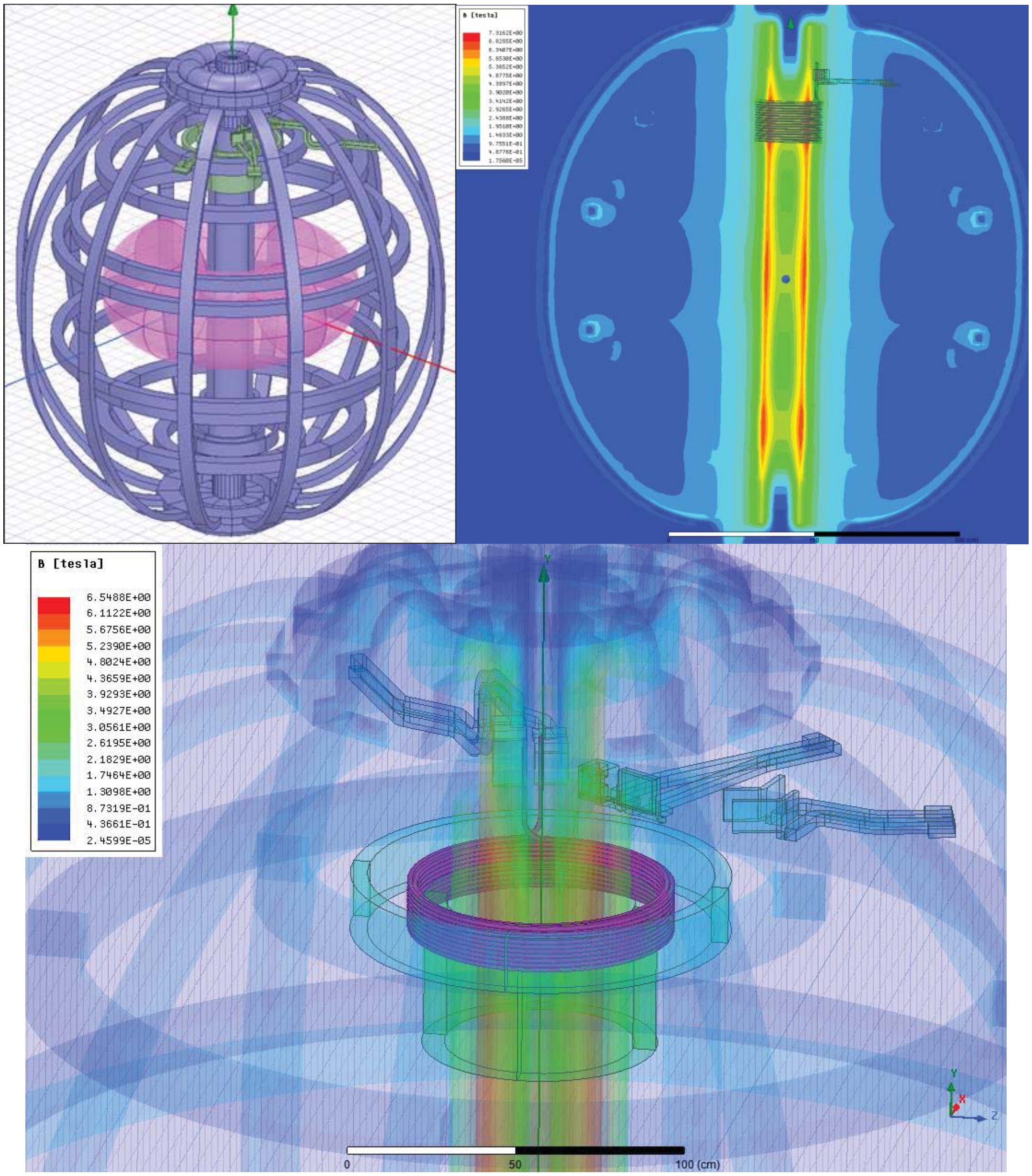

Figure 1.0-1 Global Magneto-static Analysis Models for upper inner PFs (left) and Magnetic Field Distribution for EQ #51 (right)

Table 6 – Maximum Total Magnetic Fields for Inner PFs

	PF-1a	PF-1b	PF-1c
EQ scenarios	1, 51	1, 33	18, 33
Maximum current (kA)	20	20	20
Local max B Fields (T)	2.5	3.3	3.2

The worst case EQ scenarios are selected based on the 2D scan of all 96 scenarios defined in DPSS for inner-PF coil current requirements [2]. The equilibrium scenarios of #51, #33 #18 define the maximum magnetic fields on the coil leads and full currents on coils and bus bars. Figures 5-7 present the radial field distribution on the upper inner PFs for the selected EQ scenarios. Both positive and reverse toroidal field cases are analyzed using 3D ANSYS MAXWELL and detailed structural models for leads and bus bars. Other assumptions used for lead analysis include 1) insulations are bonded to the conductors without delamination and linear elastic behavior is used for copper without yielding, 2) coil packs in 3D structural analysis have no thermal conduction with coil support structure, 3) maximum temperature of conductors at end of pulses is prescribed as defined in the 2D thermal analysis [12].

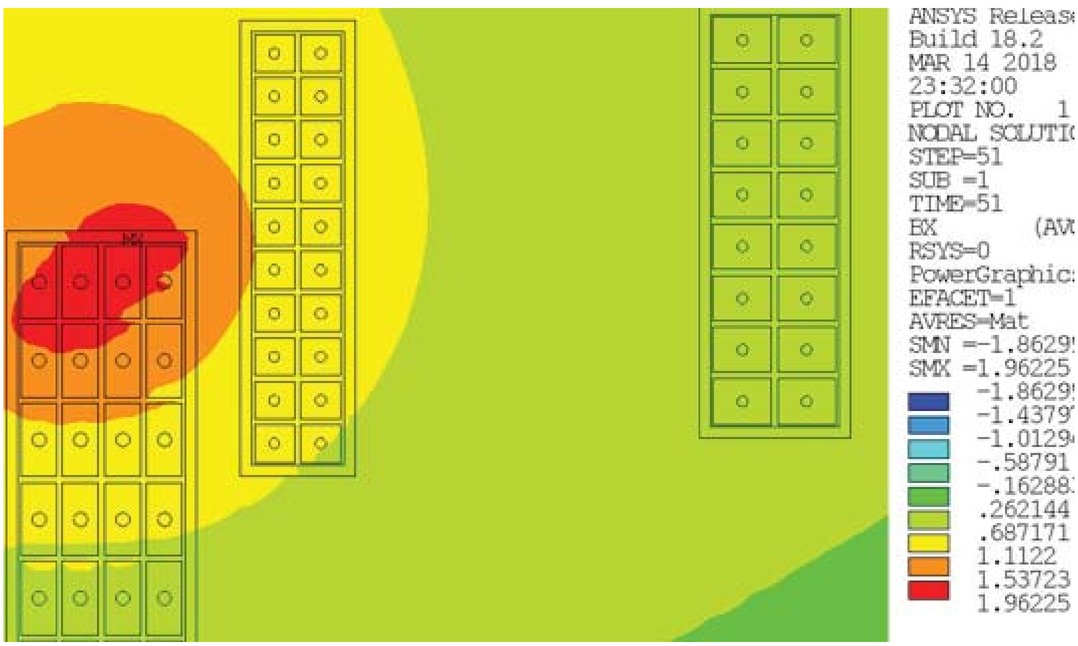

Figure 4.0-2 Radial field from EQ #51 (2 MA circular plasma) – worst for PF-1a Leads

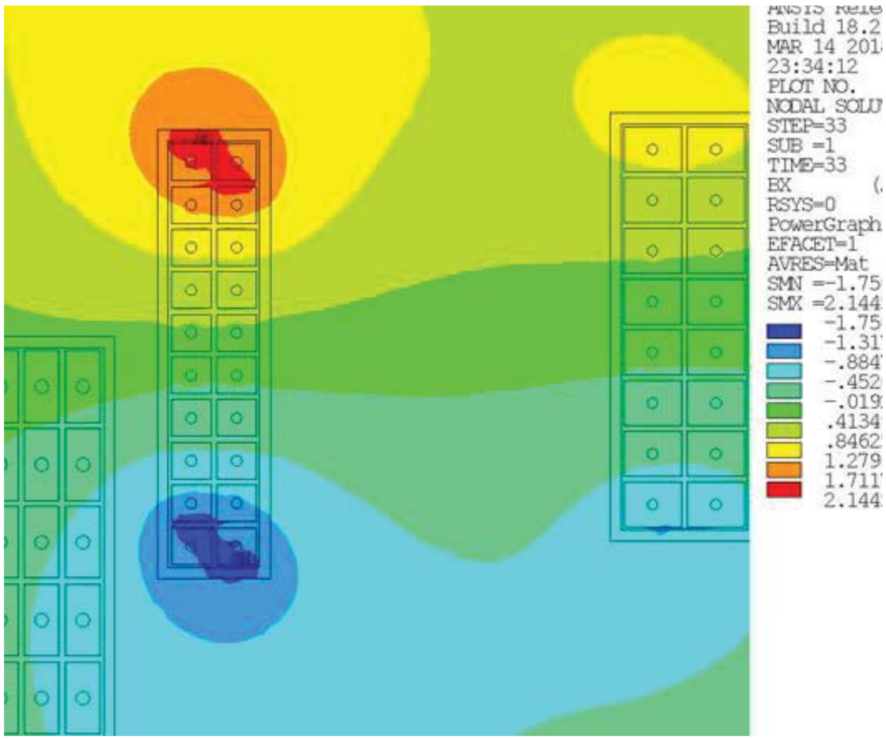

Figure 4.0-3 Radial field from EQ #33 (2 MA circular) – worst for PF-1b Leads

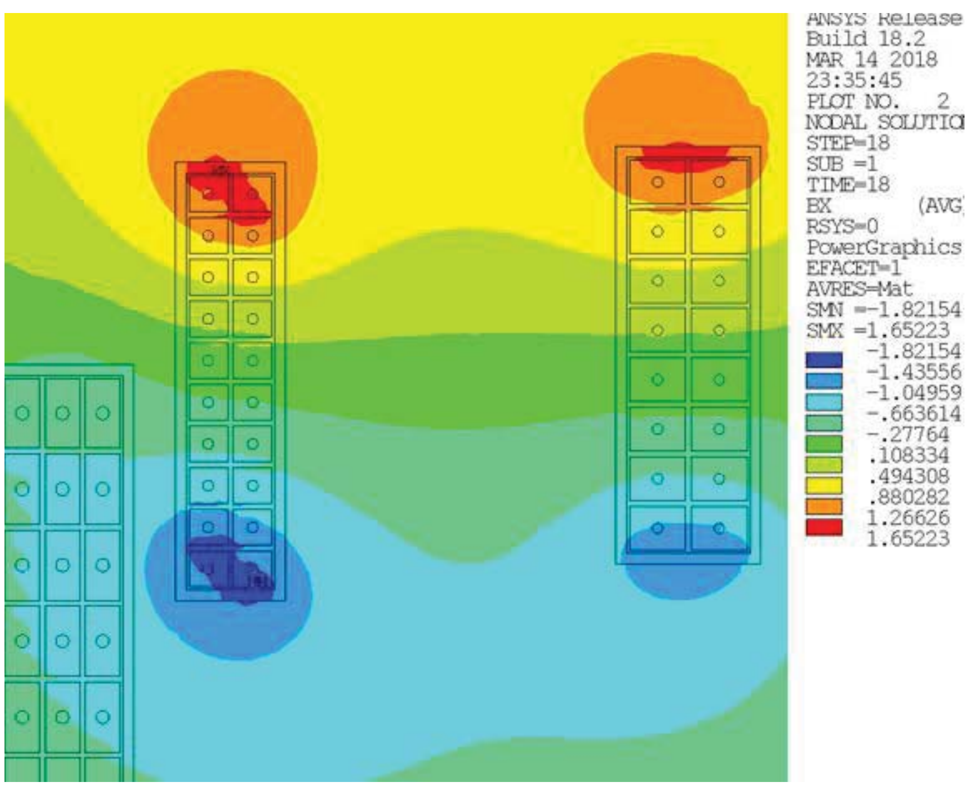

Figure 4.0-4 Radial field from EQ #18 (2 MA circular) – worst for PF-1c Leads

5. EM Results

When the inner PFs are energized, the conductor will be pulsed up to ~20 kA for about 1-2 seconds. The conductor and insulation will experience fatigue stress and strain, but thermal stress during cool down dominates the fatigue evaluation for the conductor and stress due to Lorentz loads dominates fatigue evaluation for coil leads. During normal operation, the equivalent square wave (ESW) time of PF-1a, -1b and -1c coils is 1.9, 1.0 and 1.4 seconds respectively. The net forces on inner PF coils extracted from the 3D MAXWELL models are comparable with the DPSS as shown in Table 5 below.

Table 7 – Maximum Total Magnetic Fields for Inner PFs

		Vertical Force (klbf)		
	EQ#18	DPSS	MAXWELL	%
2 MA	PF1AU	-44.46	-44.23	-0.52
circular	PF1BU	17.29	17.96	3.88
plasma	PF1CU	-4.18	-3.6	-13.88

With Plasma

PF1U Coil Vertical Force (lbf) vs Current Scenario

Coil/CS#	18	33	51
PF1A	-4.449E+04	1.016E+04	-4.948E+04
PF1B	1.760E+04	-4.159E+04	0.000E+00
PF1C	-3.891E+03	-2.613E+04	0.000E+00

Magnetic Fields and Body Forces

The magnetic field distribution on the PF-1a upper and PF-1b lower conductors and bus bars are shown in Figure 8 below for the worst case EQ scenarios (EQ #51 and #33). Figure 9 presents the detailed volume force density on the conductors and bus bars of PF-1a upper. The plot clearly indicated conductor in the solenoid is under clamping force and bulged out in the mid-plane, which is the typical behavior of solenoid magnets when energized.

The volumetric force densities for each 3D magnetostatics analysis of the worst case EQ scenarios (both positive and reverse toroidal field cases) for the inner PFs have been extracted from MAXWELL calculators and saved as the database for inputs to the static structural analysis of the coil leads and bus bars. The data are saved in a typical format of (x, y, z, Fx, Fy, Fz) and can be directly imported in ANSYS external data for structural analysis.

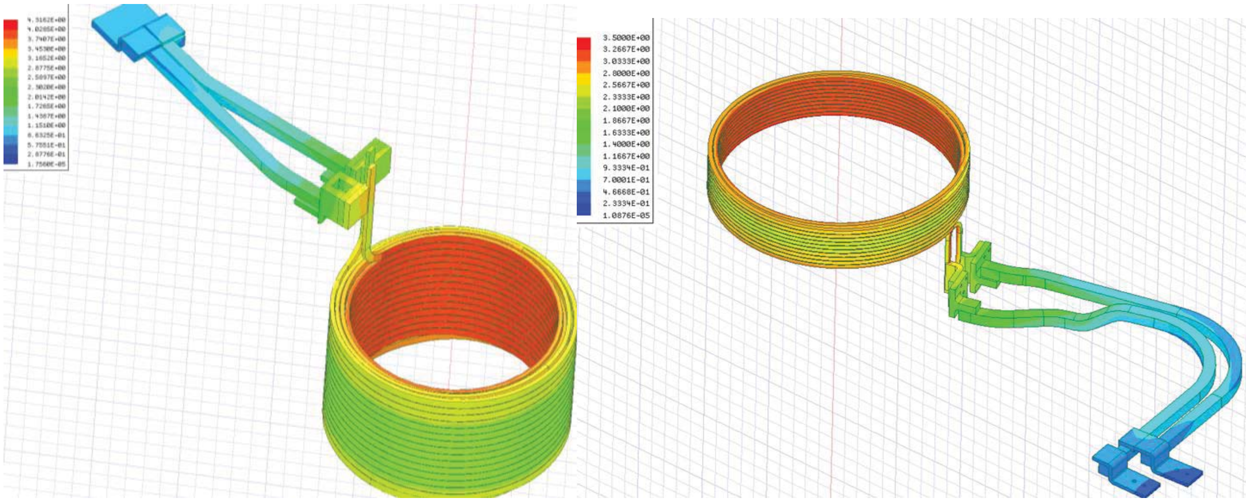

Figure 5.0-1 Total magnetic fields on PF-1a upper and PF-1b lower conductors

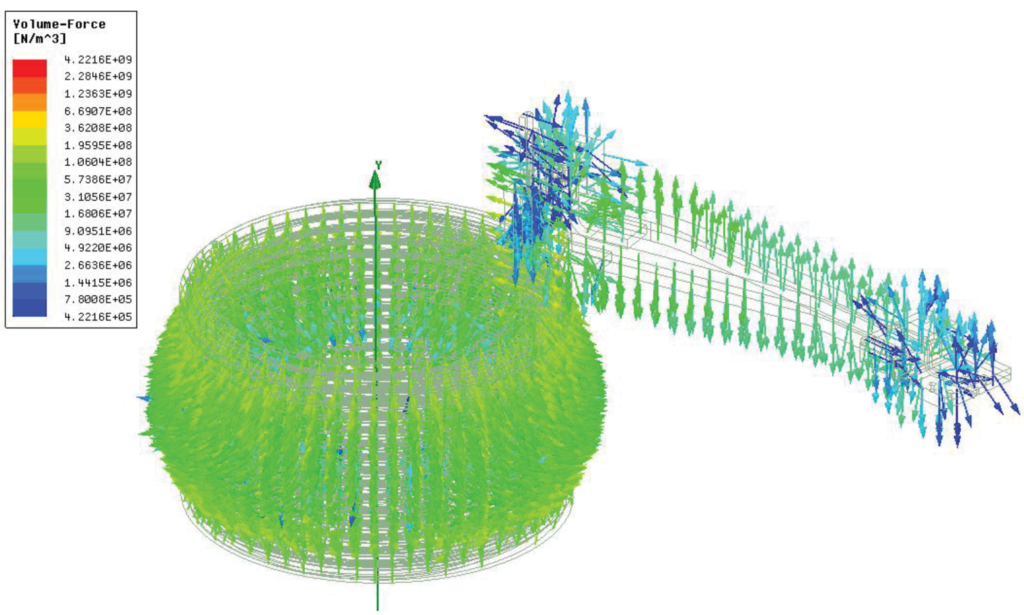

Figure 5.0-2 The body force density in PF-1a coil winding and bus bars

The volumetric body force density on the conductor and bus bars for the PF-1b lower is shown in Figure 10. The force density distribution shows very similar behavior of solenoid magnets when energized. The force density on the coil terminals is also clearly shown in Figure 10, where higher force density is expected from interaction with the significant toroidal fields. Table 6 presents the maximum local radial, vertical as well as the toroidal fields on each of the inner PF coils and coil terminals. Note that the toroidal fields can switch sign and both positive and reverse toroidal field cases are analyzed for the coil leads for each inner PFs.

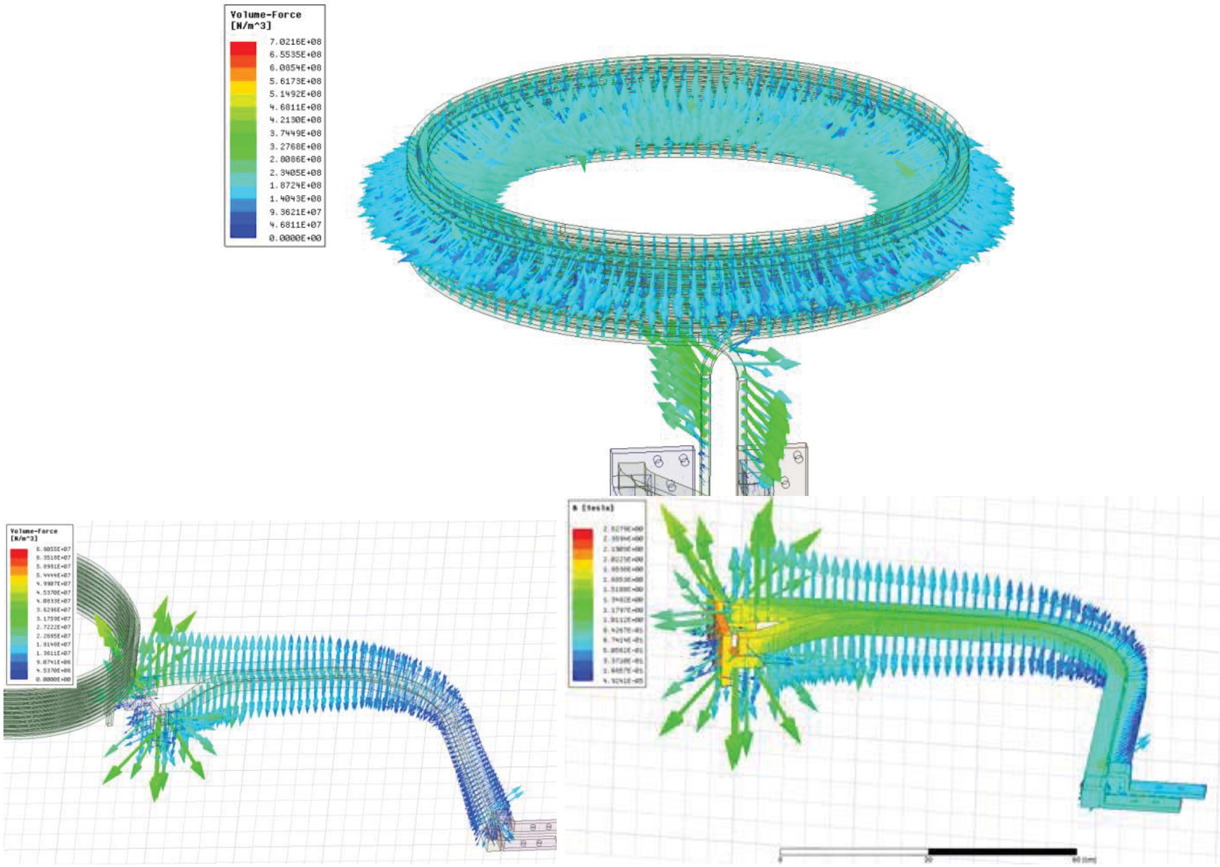

Figure 2 PF-1b lower body force distribution on conductor and bus bars EQ#33.

Table 8 – Maximum Fields on Inner PF Coils

	PF-1a	PF-1b	PF-1c
Worst EQ #	51	18, 33	18
Radial B_r (T)	2	2.1	1.7
Vertical B_z (T)	2.5	2.2	1.1
Toroidal B_t (T)	2.9	2.4	1.7

Mapping of Elemental Body Force Density

For the analysis of PF1a,b,Upper and lower forces were mapped directly from Maxwell to Workbench. For PF1cU and L intermediate “Cloud Data” files were generated . This is also explained in reference [18]. A typical format of the body force density as input to the structural analysis is shown below. All input files are assembled and stored on the google drive folder. Figure 11 presents the body force densities mapped onto the structural models for the PF-1a and PF-1b upper assembly and the PF1b lower assembly. Figure 11 clearly shows the higher force density on the coil terminals as result of the impact from the toroidal field which is quite significant for the coil terminals. Table 7 presents the typical volumetric force density extracted from the 3D MAXWELL run (PF1CL EQ18).

Table 9 – Typical Volumetric Force Density Extracted from MAXWELL

X (m)	Y (m)	Z (m)	Fx (N/m^3)	Fy (N/m^3)	Fz (N/m^3)
-5.76E-01	-1.85E+00	1.02E-02	6.25E+07	4.03E+07	8.34E+05
-5.66E-01	-1.84E+00	1.00E-02	2.66E+07	3.02E+07	7.10E+05
-5.76E-01	-1.84E+00	1.02E-02	6.46E+07	2.82E+07	4.96E+05
-5.66E-01	-1.85E+00	7.52E-03	2.49E+07	4.24E+07	1.05E+06
-5.56E-01	-1.84E+00	9.85E-03	-9.39E+06	2.02E+07	5.86E+05
-5.66E-01	-1.84E+00	1.00E-02	2.86E+07	1.81E+07	3.72E+05
-5.56E-01	-1.84E+00	7.35E-03	-1.11E+07	3.24E+07	9.25E+05
-5.76E-01	-1.84E+00	1.02E-02	6.66E+07	1.60E+07	1.58E+05
-5.66E-01	-1.84E+00	7.52E-03	2.69E+07	3.03E+07	7.11E+05
-5.56E-01	-1.85E+00	4.84E-03	-1.27E+07	4.46E+07	1.26E+06

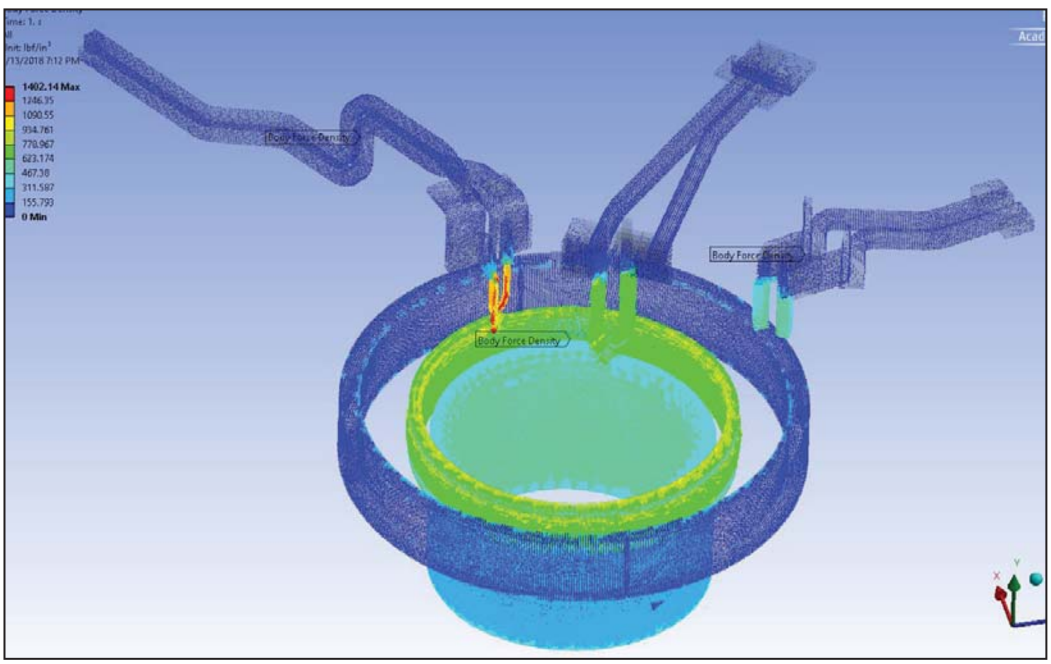

Figure 5.0-4 PF1bU Force Density Plot

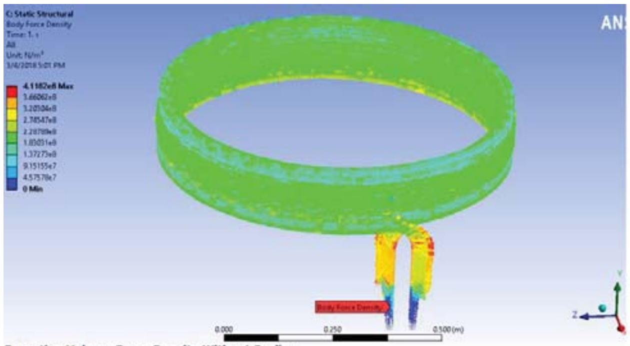

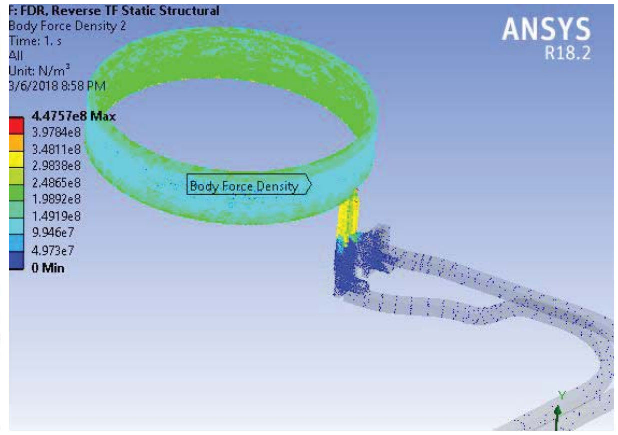

Exporting Volume Force Density Without Scaling...

Object	Total Force From Maxwell 3D	Total Force Mapped	Ratio
Box2	(0N, 0N, 0N)	(0N, 0N, 0N)	0
EDC111001	(-465.311N, 160012N, -1073.12N)	(87.9021N, 149253N, -1930.91N)	1.07203

Figure 3 PF-1b Lower - Mapped Force Density on Coils

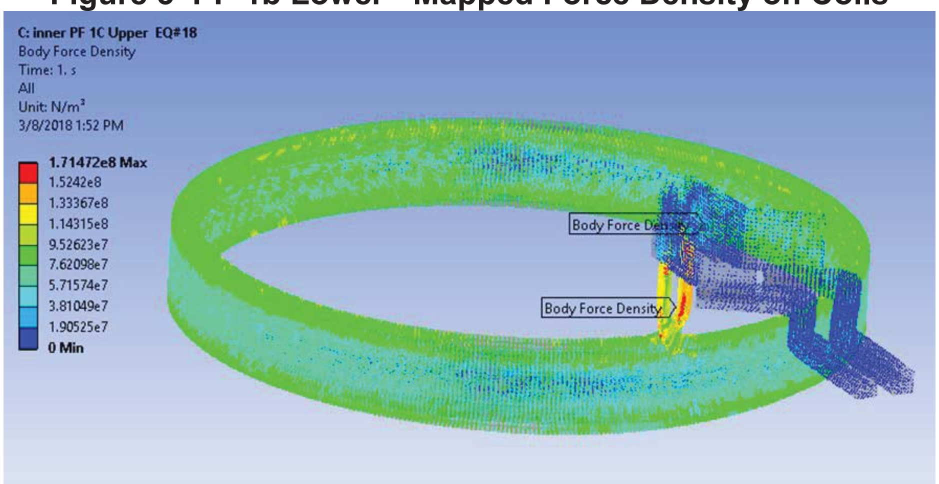

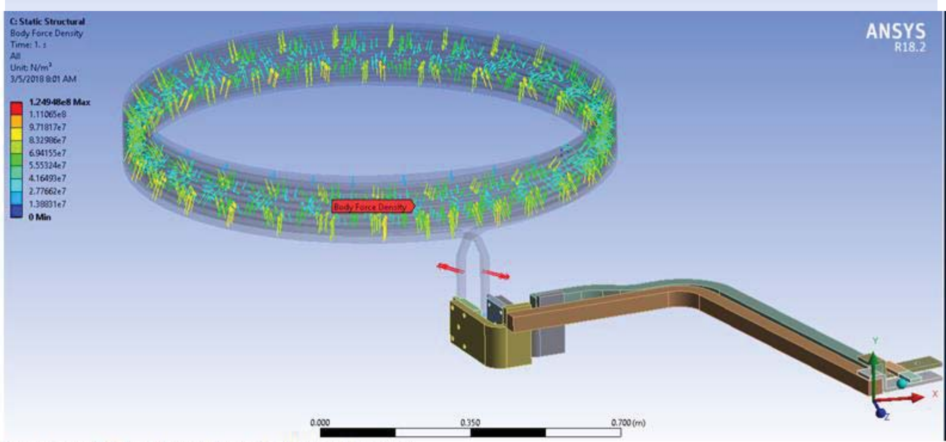

Exporting Volume Force Density Without Scaling...

Object	Total Force From Maxwell 3D	Total Force Mapped	Ratio
Box2	(0N, 0N, 0N)	(0N, 0N, 0N)	0
EDC111011_body4	(71.802N, 116833N, -1561.96N)	(-187.639N, 115926N, -9439.08N)	1.00459

Figure 5.0-6 PF-1b Lower - Mapped Force Density on Coils

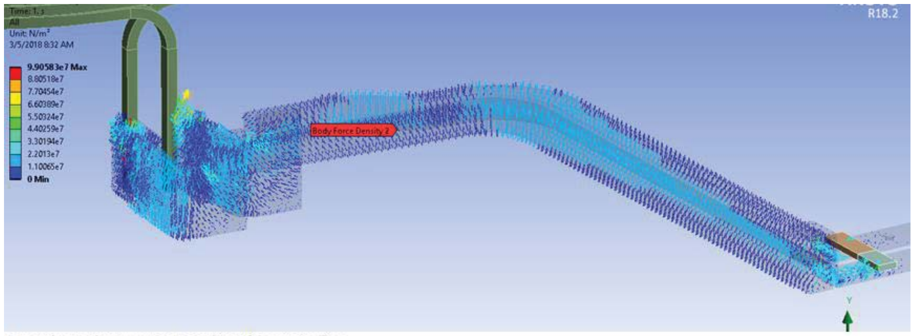

Exporting Volume Force Density Without Scaling...

Object	Total Force From Maxwell 3D	Total Force Mapped	Ratio
Box2	(0N, 0N, 0N)	(0N, 0N, 0N)	0
JWPF1CLOWER1BUSFLAG	(-390.138N, 3363.89N, -1629.96N)	(-381.566N, 3383.37N, -1624.52N)	0.996229
JWNEWPF1CLOWER2	(-3730.41N, -15670.4N, 4920.93N)	(-3727.78N, -15659.6N, 4918.95N)	1.00066
JWPF1CLOWER2BUSFLAG	(-294.811N, -5216.82N, 1774.65N)	(-297.711N, -5207.71N, 1760.05N)	1.00239
EDC14724	(554.404N, 1668.05N, 384.135N)	(557.029N, 1680.2N, 385.674N)	0.993152
EDC14724_1	(-555.141N, -1752.91N, -632.248N)	(-555.715N, -1734.27N, -630.528N)	1.00892

Figure 5.0-7 Force Density Plot

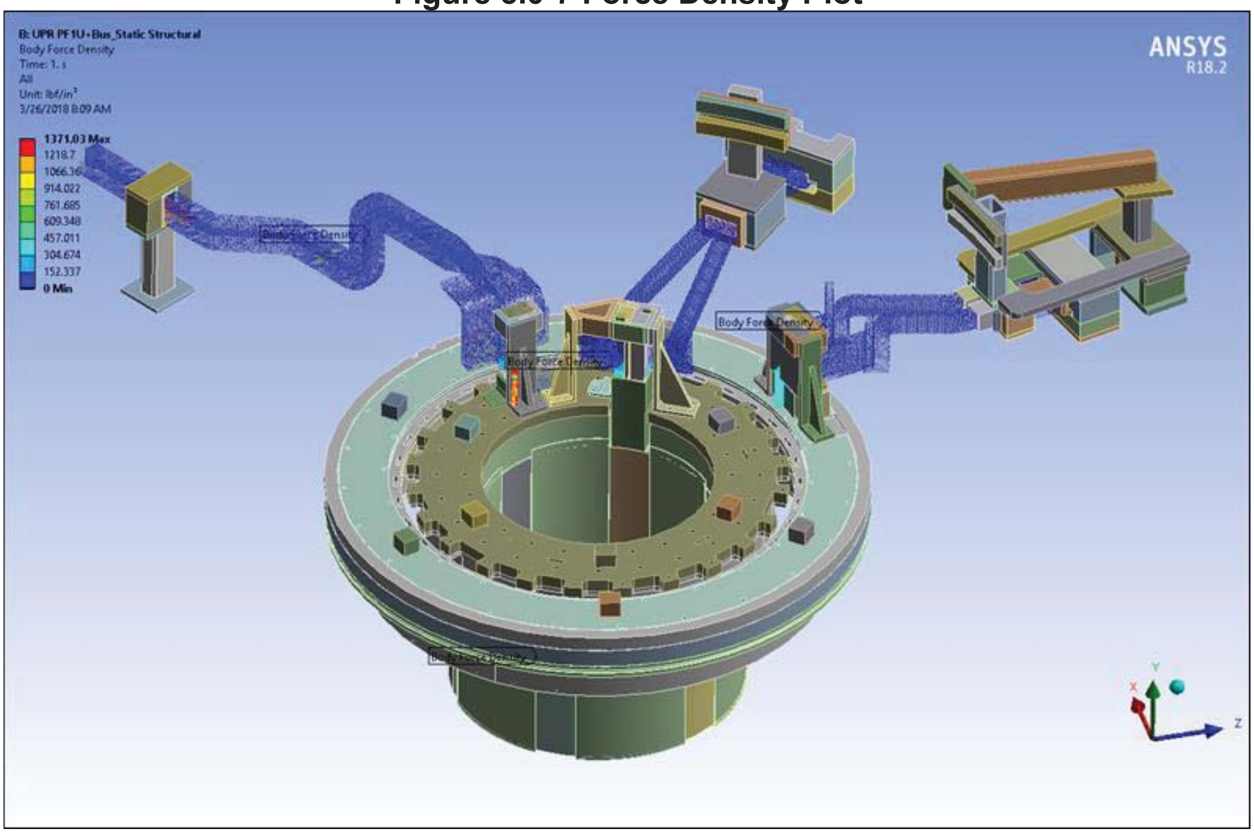

Figure 5.0-8 Force Density Plot Upper Bus

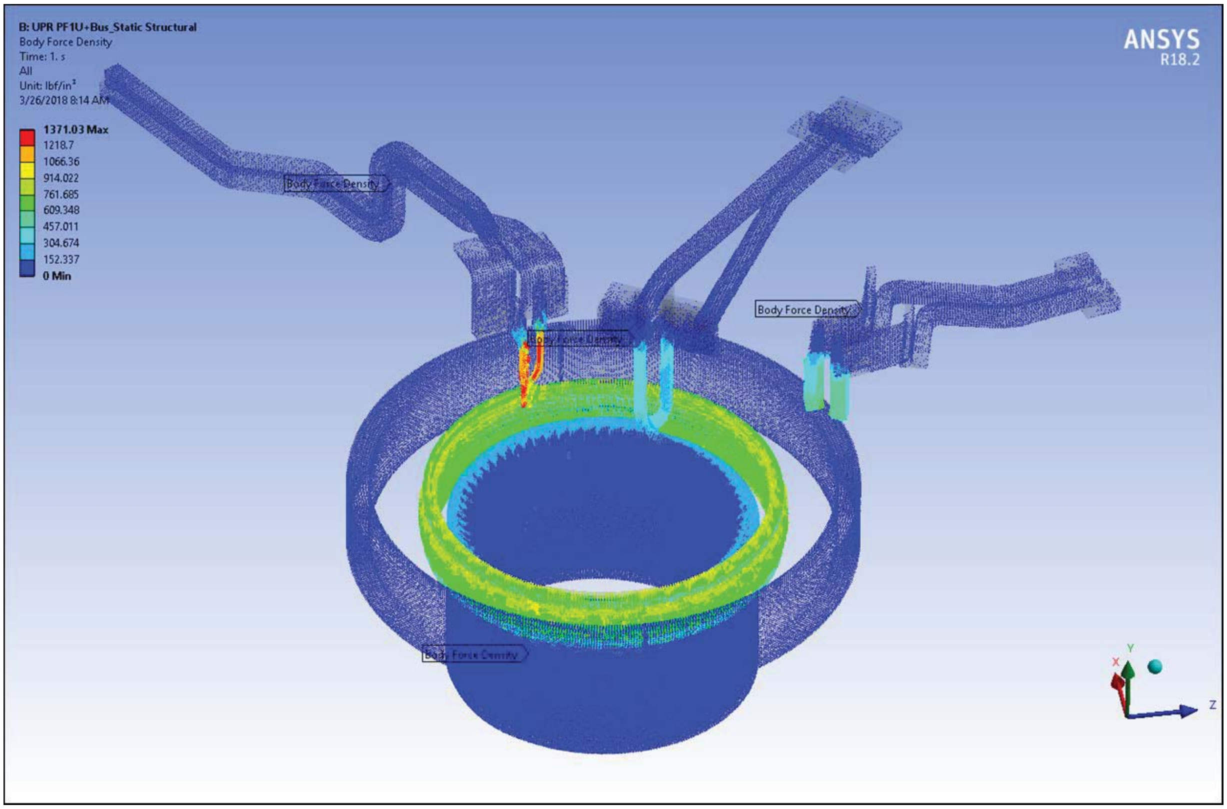

Figure 5.0-9 Coil Force Density Plot

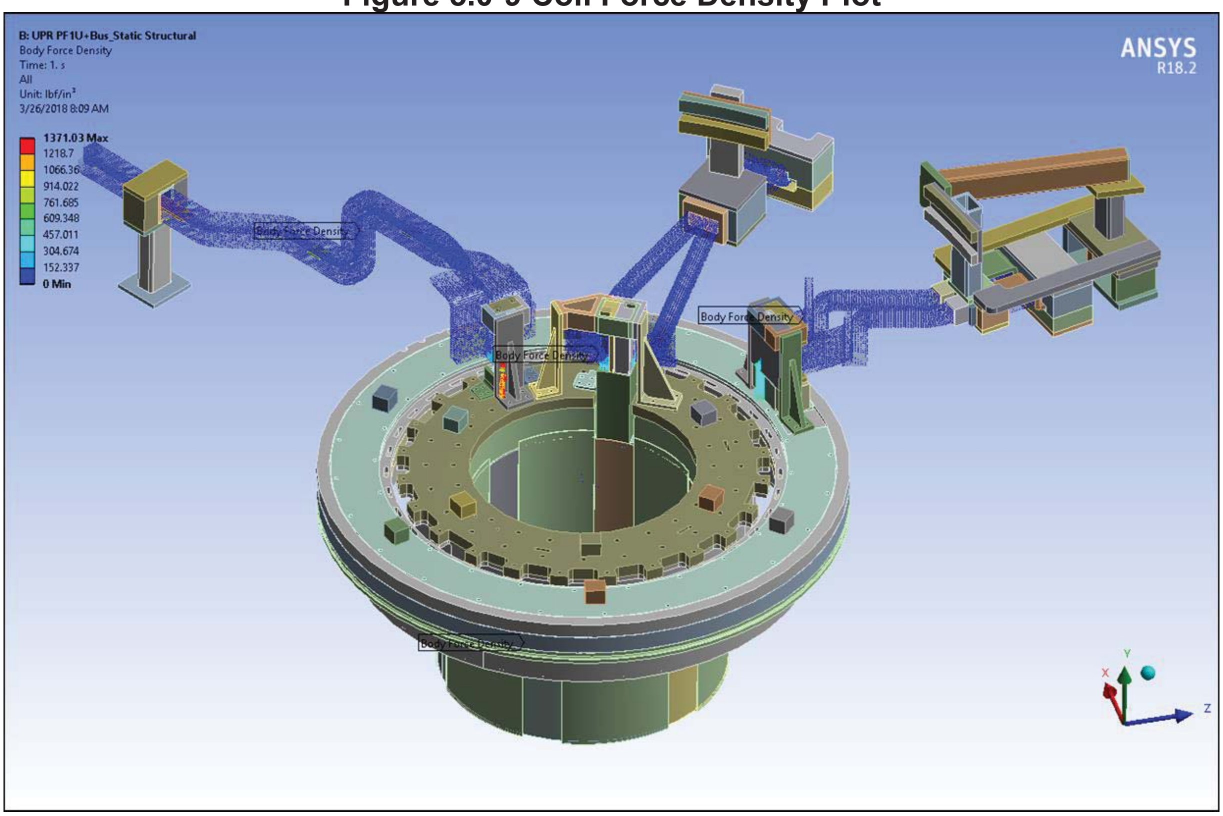

Figure 5.0-10 PF-1c upper and lower conductor and bus bar mapped force density

6. Structural Analysis Results

ANSYS WorkBench Project Page

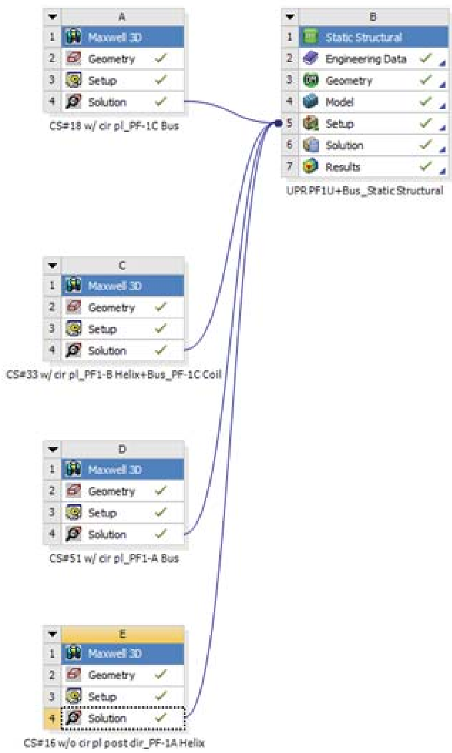

ANSYS WorkBench Project Page

Table of Worst-Case DPSS Scenarios

Coil	Scenario #	
	Bus Bar	Coil Lead
PF-1A	51	16
PF-1B	33	33
PF-1C	18	33

Figure 6.0-1

When the inner PFs are energized, the conductor will be pulsed up to ~20 kA for about 1-2 seconds. The conductor at coil terminals will experience thermal as well as EM fatigue stress and strain, but thermal stress during cool down dominates the fatigue evaluation for the conductor and stress due to Lorentz loads dominates fatigue evaluation for coil leads. Structural analysis of the coil leads is divided into 3 groups 1) PF-1a and PF-1b upper structural assembly; 2) PF-1a and PF-1b lower structural assembly; 3) PF-1c upper and lower lead and bus bar analysis. Figure 13 below shows the typical finite element meshes used in the structural analysis model for the PF-1a and PF-1b upper lead analysis.

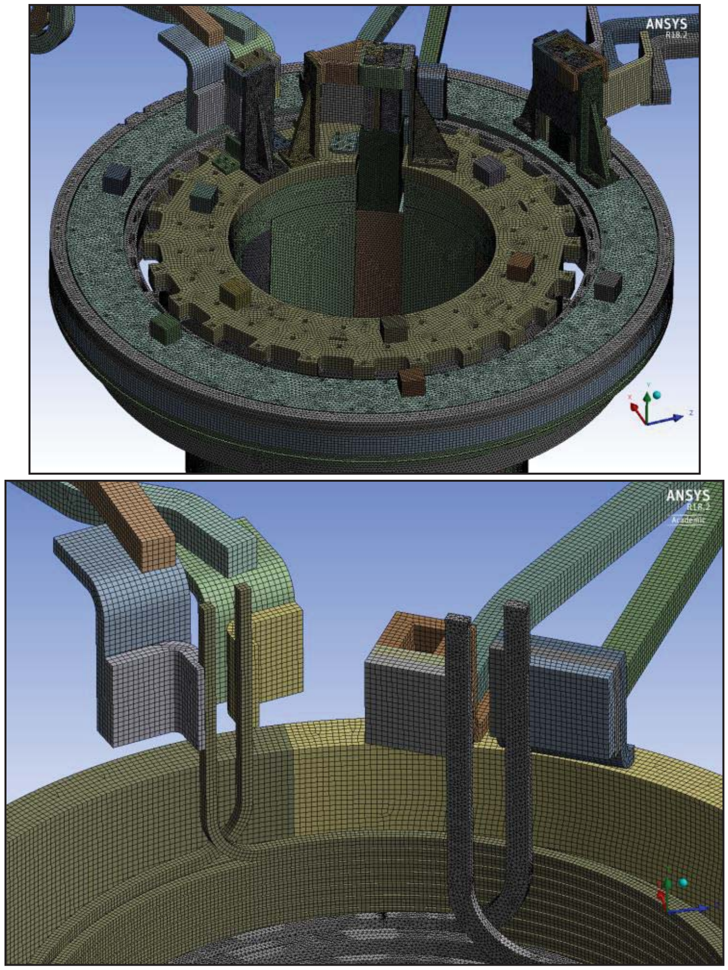

Figure 4 Detailed Mesh used for the PF-1a and PF-1b lead analysis

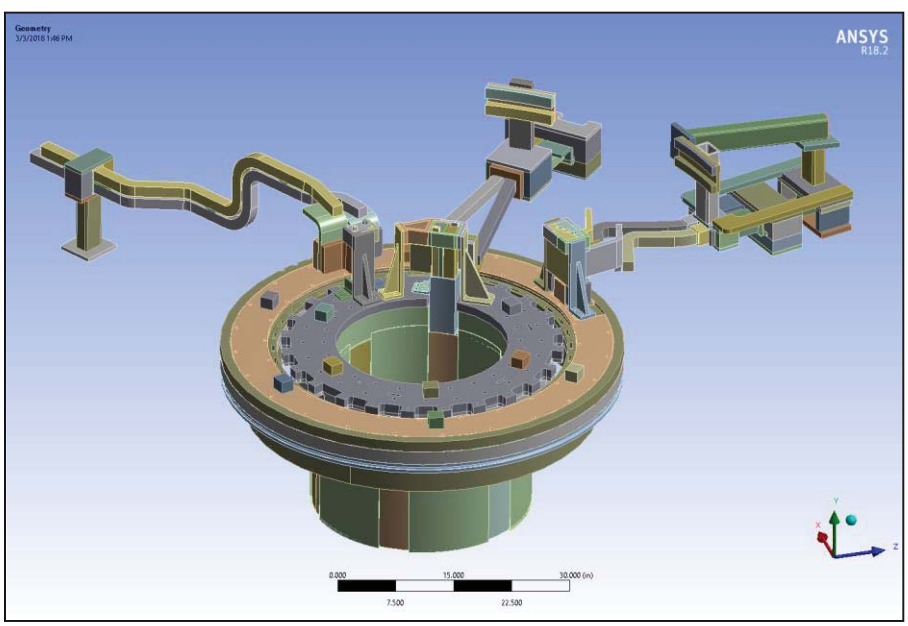

Figure 6.0-3 Upper Polar Region Solid Model Part Color

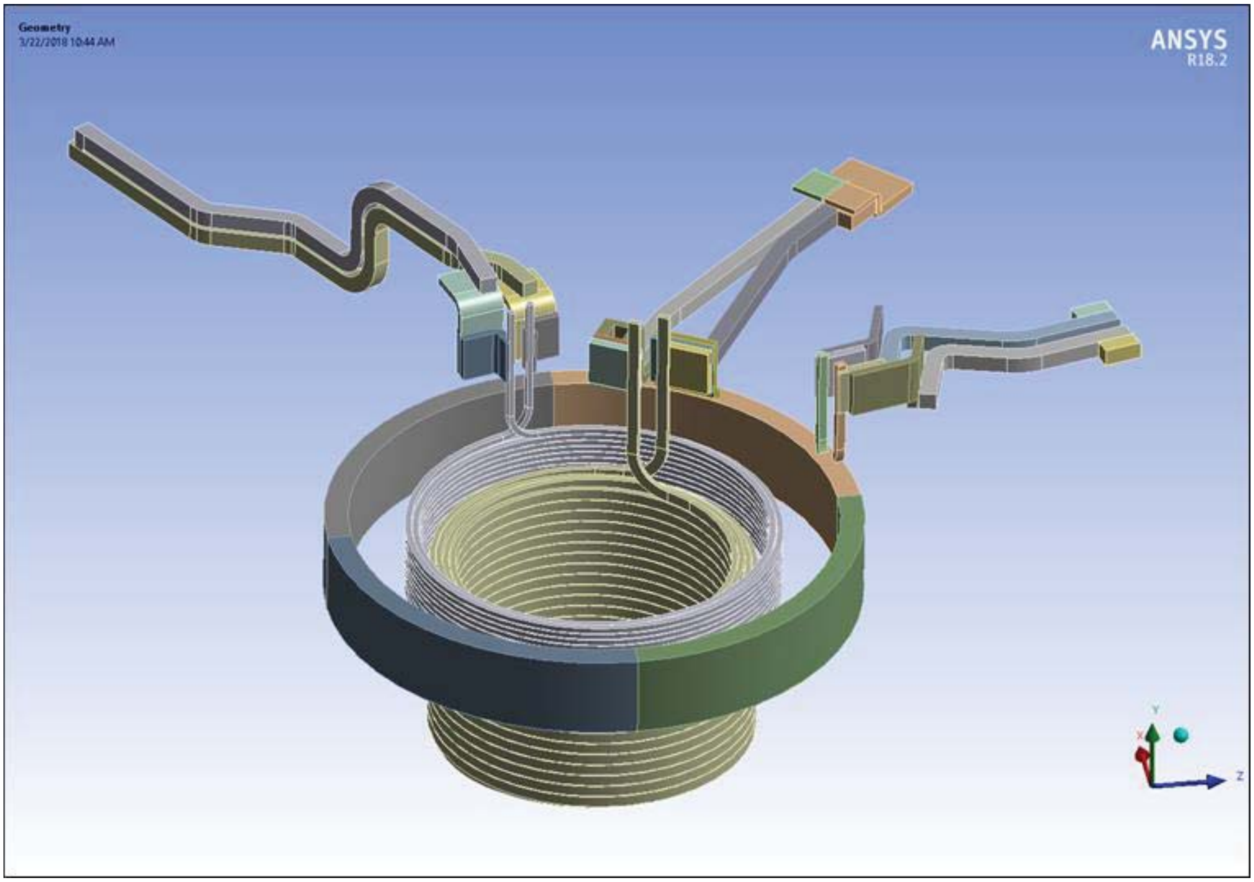

Figure 6.0-4 PF-1A, PF-1B, PF-1C Conduction Paths

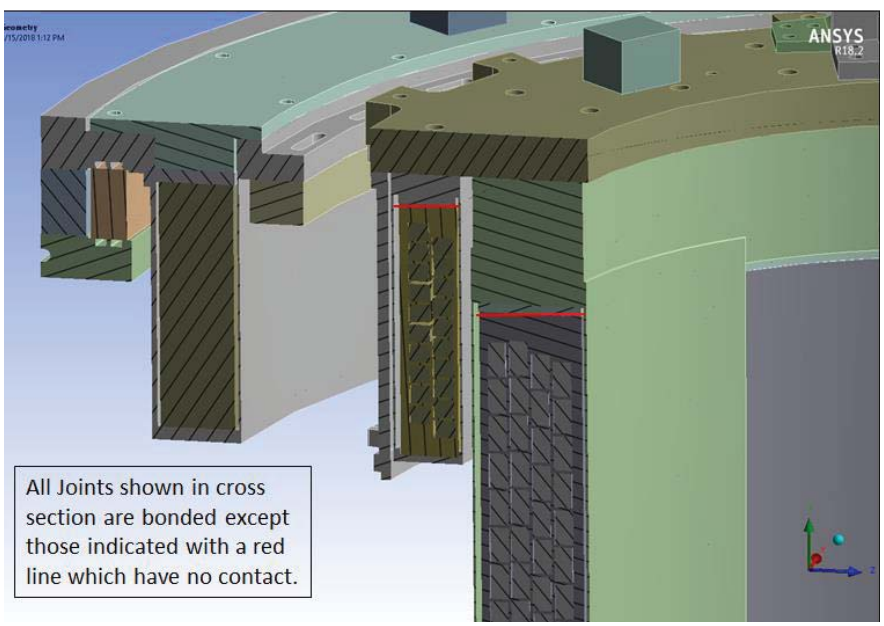

Figure 6.0-5 Upper Polar Region Solid Model Part Color Contact Modeling

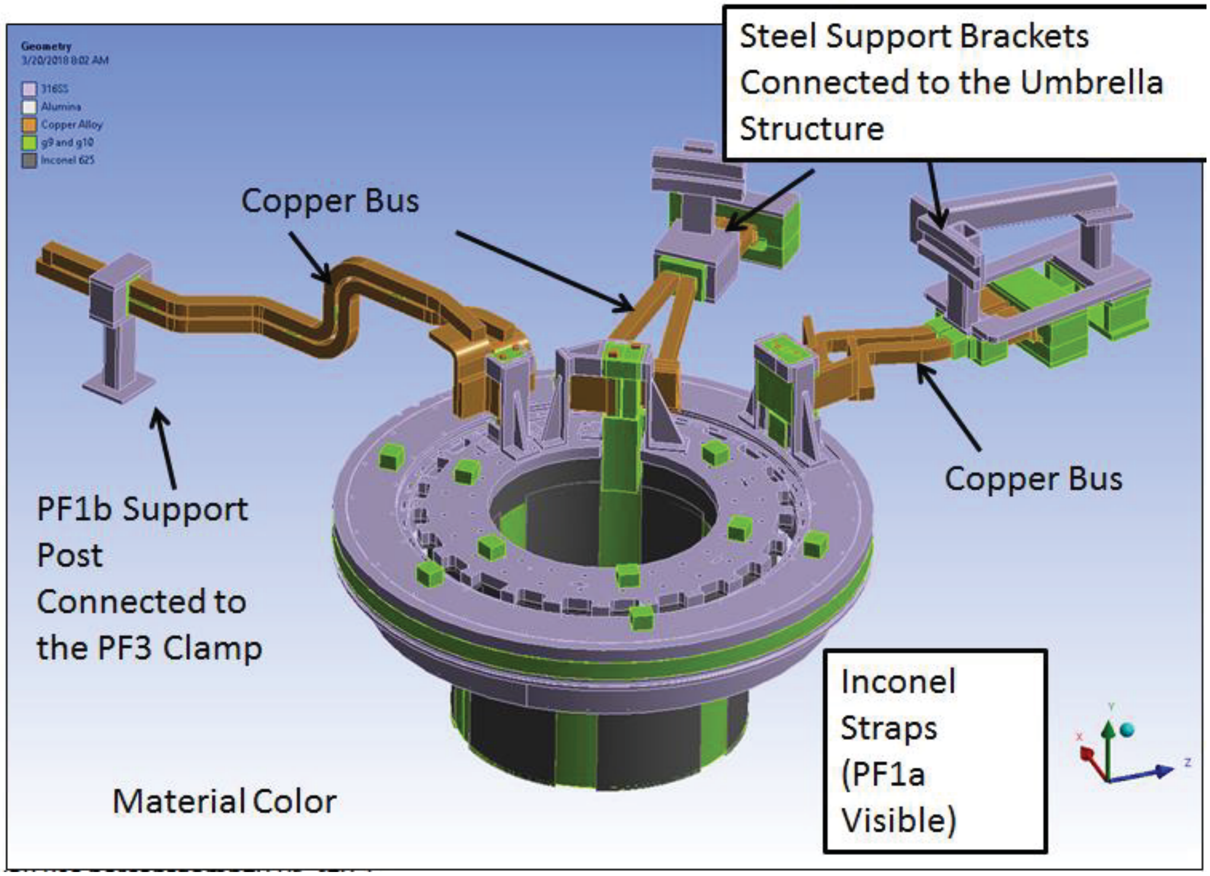

Figure 6.0-6 Upper Polar Region Solid Model, Material Color

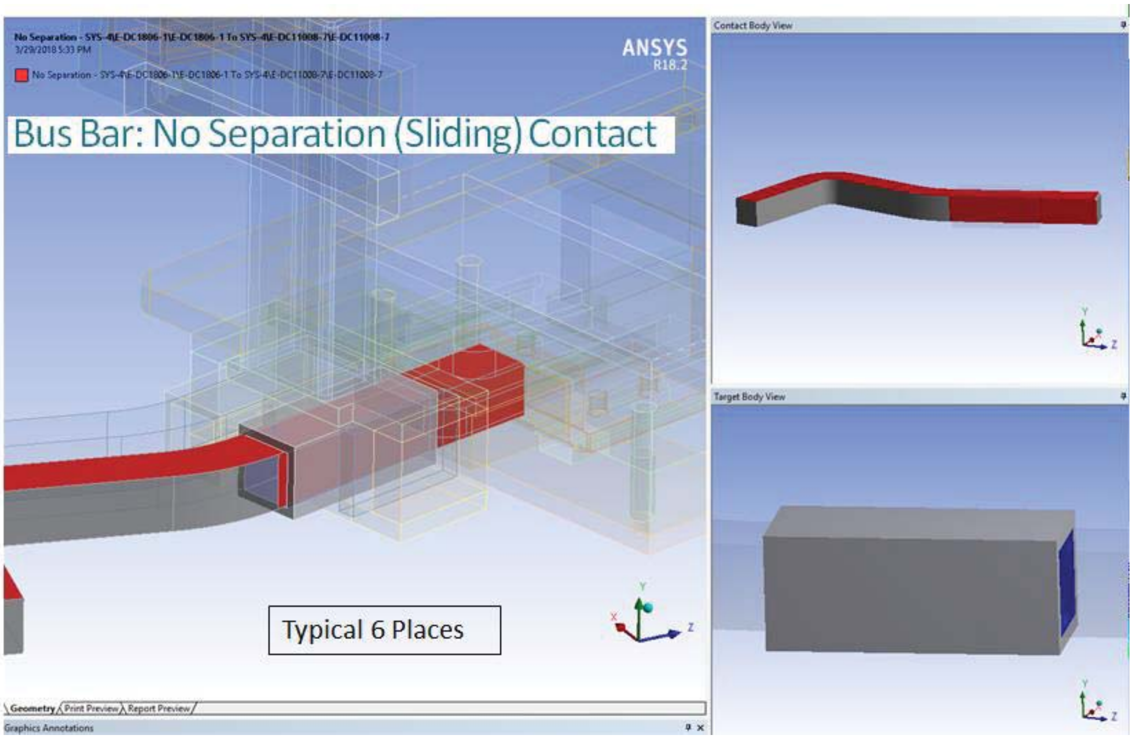

Figure 6.0-7 Upper Polar Region Solid Model, Bus Bar Interface Elements

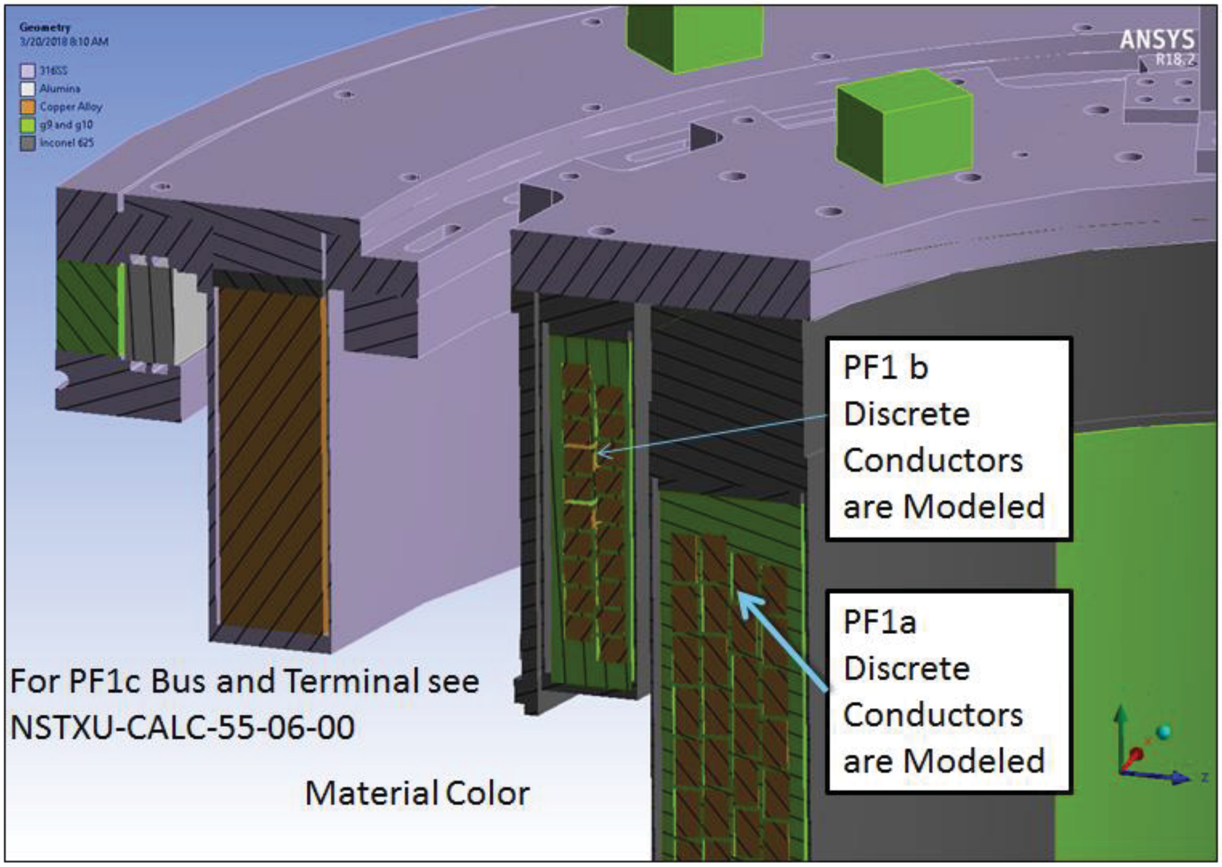

Figure 6.0-8 Winding Pack Modeling

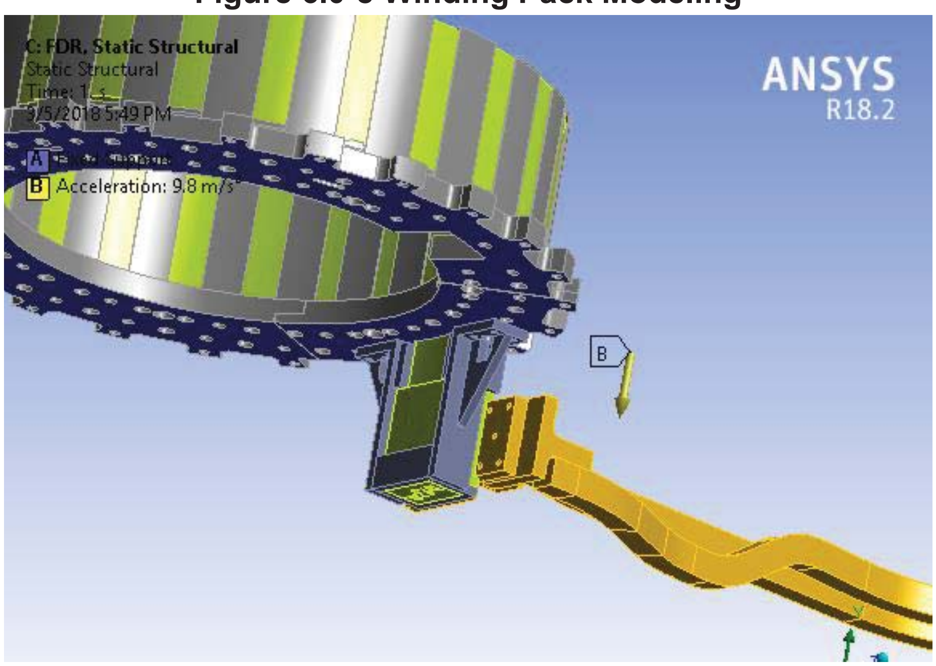

Figure 5 PF-1b Lower coil, coil terminal and bus bar assembly

Previous analysis indicates that structural support of the conductor at coil terminals is critical to ensure stress level at terminals is within the fatigue design limit. To this end, support structures such as the G10 filler blocks, support brackets as well as bus bars are redesigned for all six coil leads based on the in-field measurements to meet space constraint. Figure 6.0-9 presents the PF-1b lower coil terminal and bus bar assembly for the lead analysis.

Preload is required for PF-1a and PF-1b coils to maintain coil structural integrity when local insulation delamination occurs during the cool down period. Figure 15 presents the Preload mechanism implemented into the coil support structure design for the PF-1a and PF-1b coils to minimize the insulation tensile strain during cool down. The Belleville washer stack is used to ensure constant pre-load on coils. During operations when coils are energized, there will be some vertical movement as result of the lunching or centering forces on coils. To take into account this effect, springs that connected to the pressure plate are implements into the lower PF-1a and PF-1b lead analysis models. A stiffness of 2.5×10^8 N/m and length of 15 mm springs were defined in the model setup for structural analysis of the leads. The lead in and lead out sections are bonded to the copper terminal flags, as well as the G10 filler blocks in the lead support tower / bracket structures. A temperature of 30 C on the bus bars, 50 C on the terminal flags and 60 and 90 C on the PF-1a and PF-1b coils are prescribed as thermal conditions in the structural analysis of the leads. Results from the latest structural analysis of the coil sling supports indicate a potential 0.4 mm vertical motion of coils inside the sling that may affect the lead stress. Pending on a clearer definition of the motion under what load case, the spring constant can be adjust accordingly to take into this effect accurately.

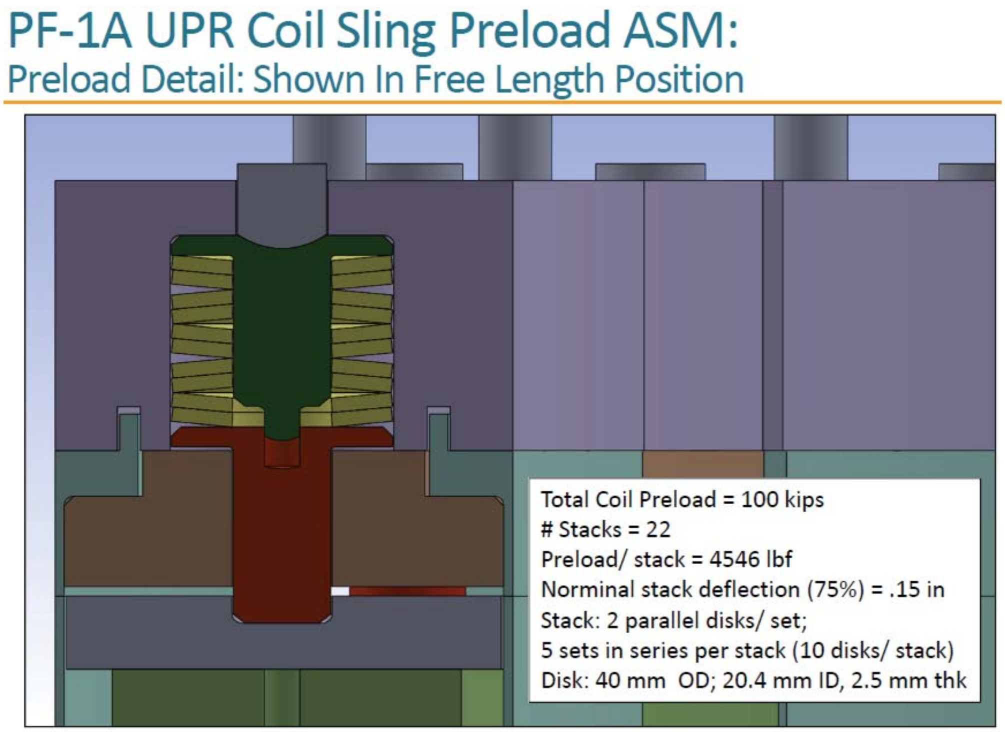

Figure 6 PF-1b Lower coil, coil terminal and bus bar assembly

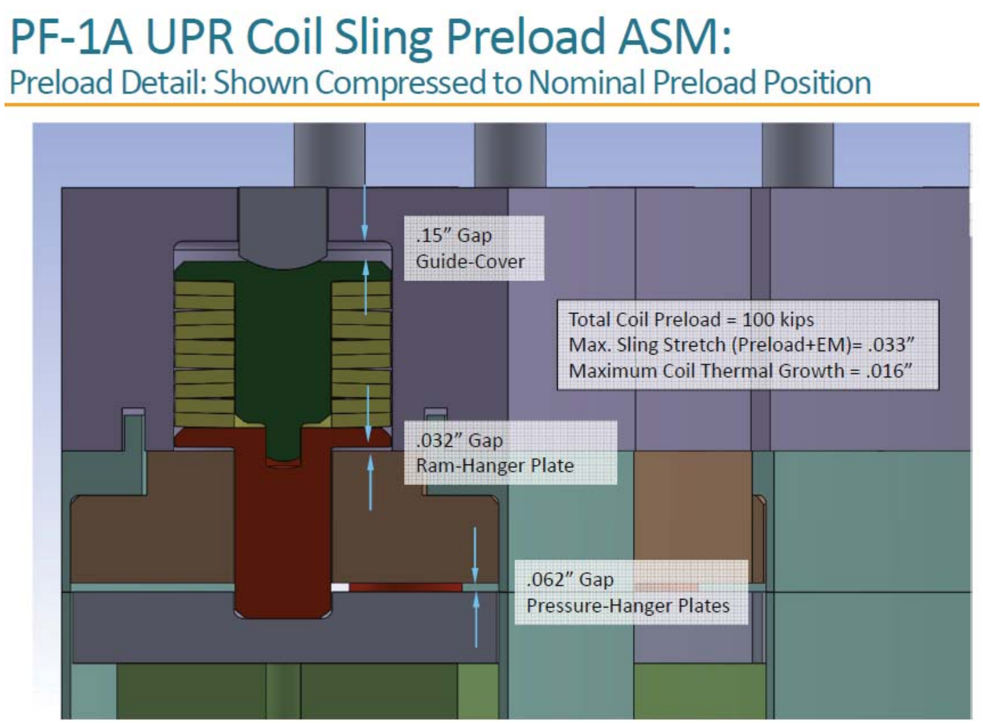

Figure 7 PF-1b Lower coil, coil terminal and bus bar assembly

6.1 PF-1a and -1b Upper Leads and Bus Bars

The PF-1a and PF-1b upper coil assembly will move 5 mm relatively to the vacuum vessel as results of center stack casing displacement during bake out [?]. Figure 17 presents the typical displacement from the PF-1a and -1b structural model assembly. Figure 18 presents the typical stresses from the PF-1a and -1b structural assembly. The coil terminals are bonded to the filler blocks but the coil pack is assembled to be able to move radially due to thermal growth. A temperature of 60 and 90 C are prescribed for PF-1a and PF-1b coils respectively. The bus bars are supported on the brackets but with possible sliding within the clamp holder.

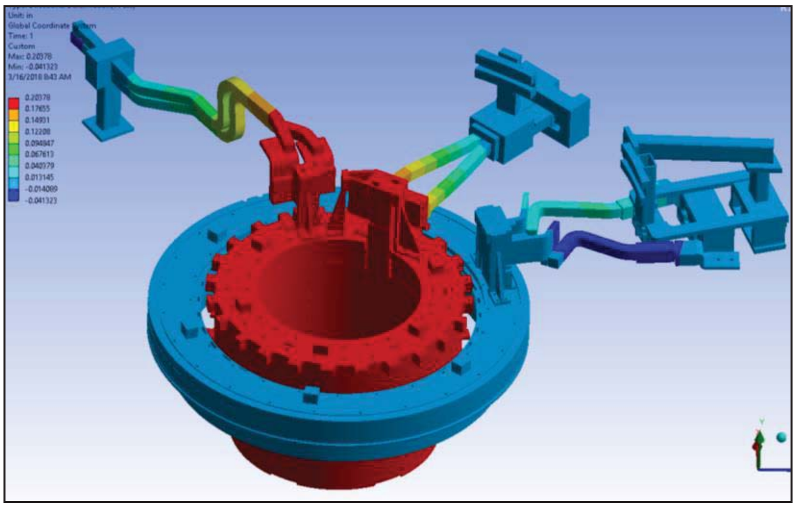

Figure 8 Displacement from PF-1a-1b structural model assembly 20 Shot Full Power Day .203 inches, 5 mm

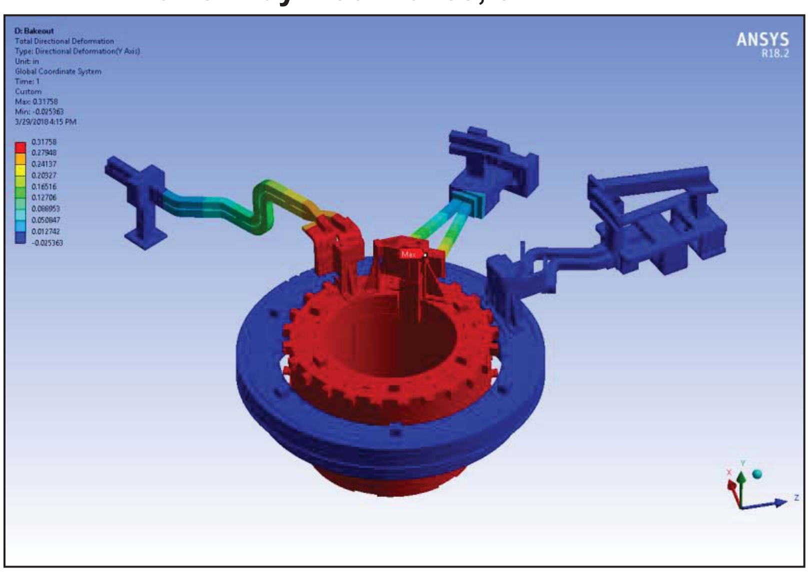

Figure 9 Vertical Displacement PF-1a-1b structural model assembly .31 in 7.87 mm

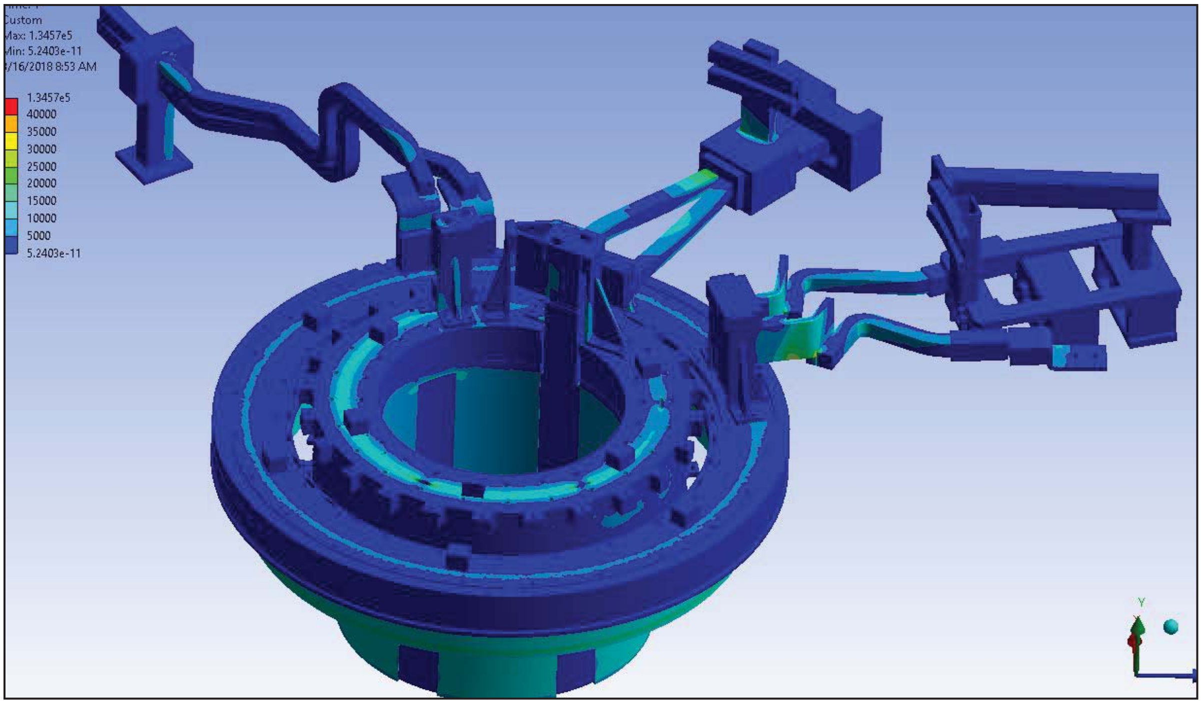

Figure 10 Stresses from PF-1a and PF-1b structural model assembly (Willard)

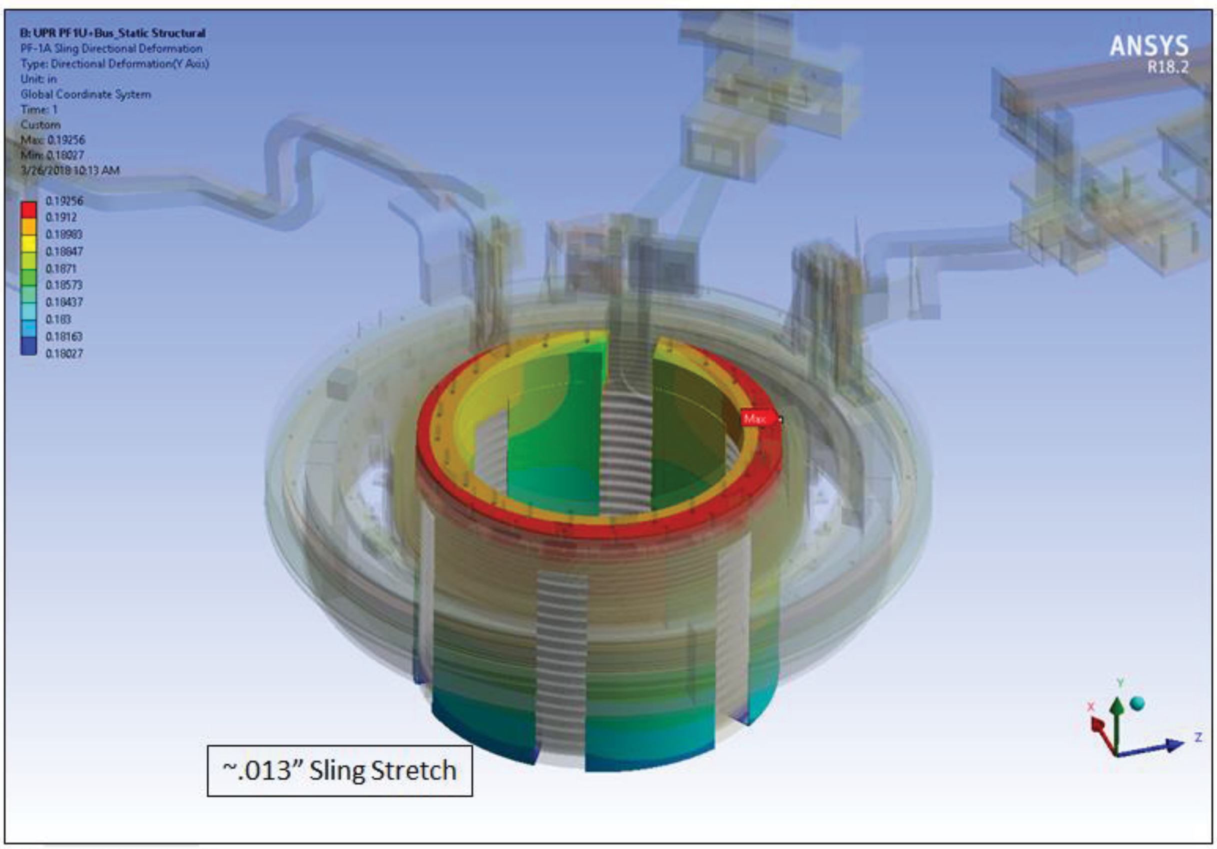

Figure 6.1-4 Y (Vertical) Displacement in inches Due to a 20 Full Power Shot Day

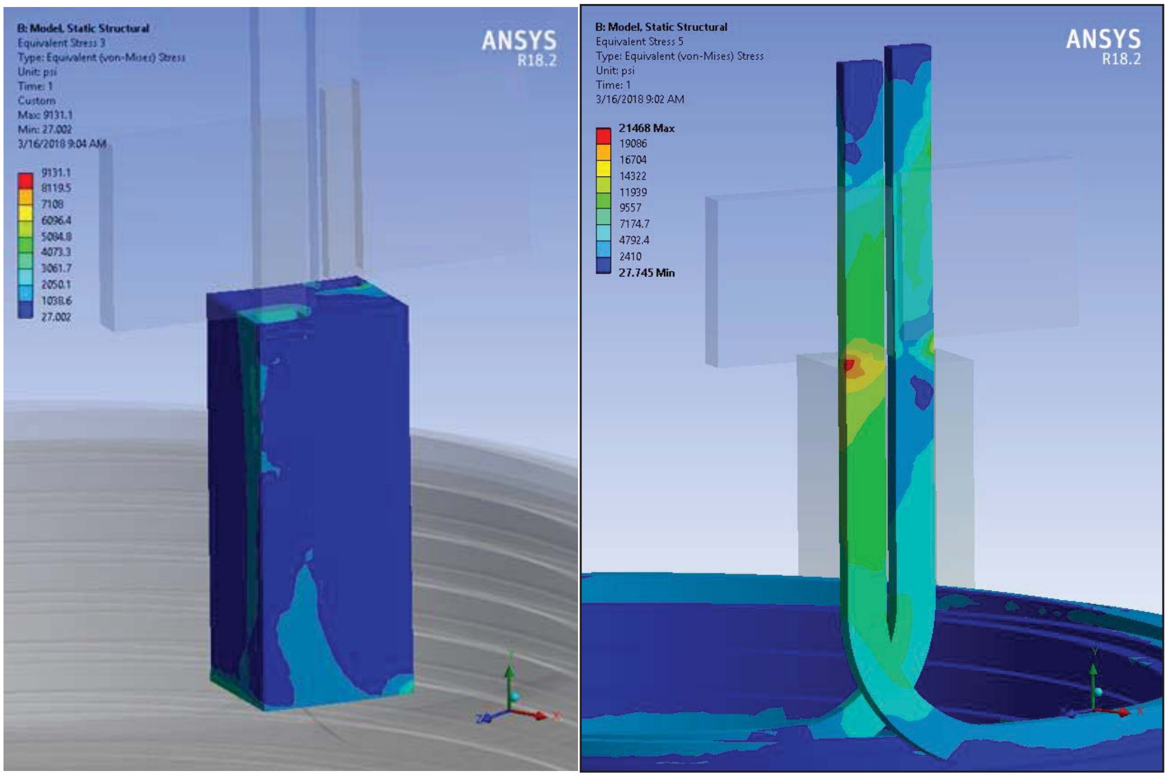

Figure 6.1-5 Stresses from PF-1a upper conductors – Peak at ~148 MPa (Willard)

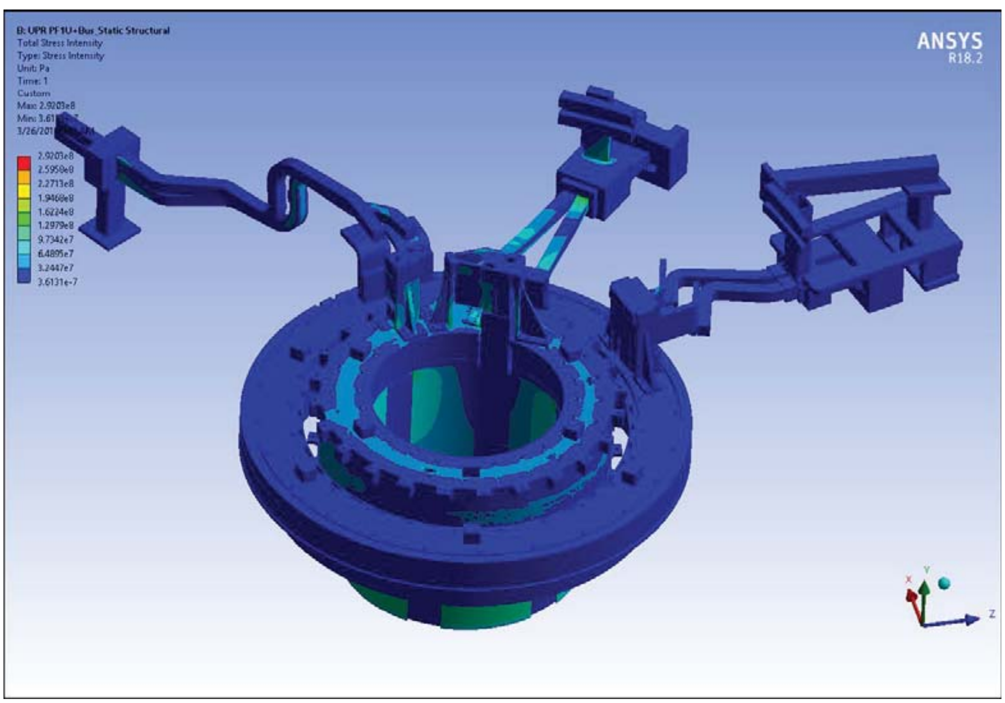

Figure 6.1-6 Stress in Full Mode

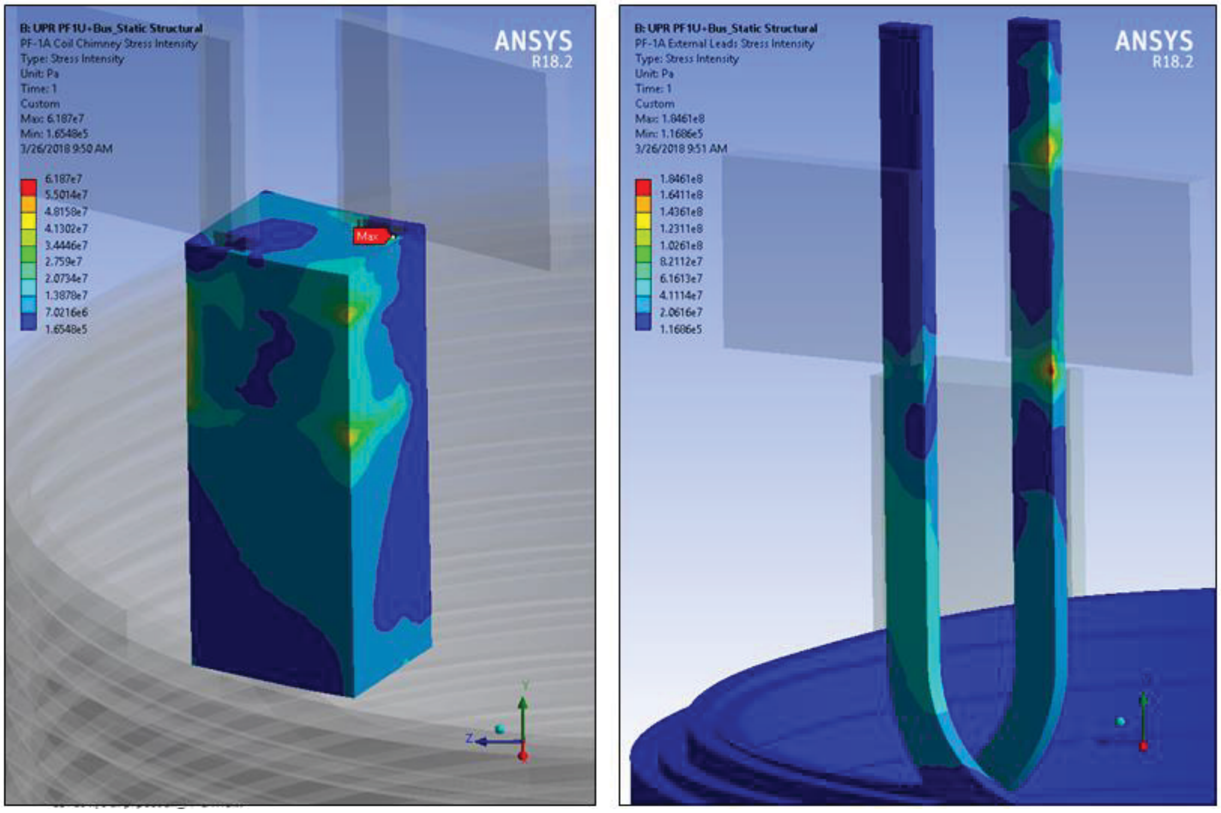

Figure 6.1-7 Lead Tresca Stress

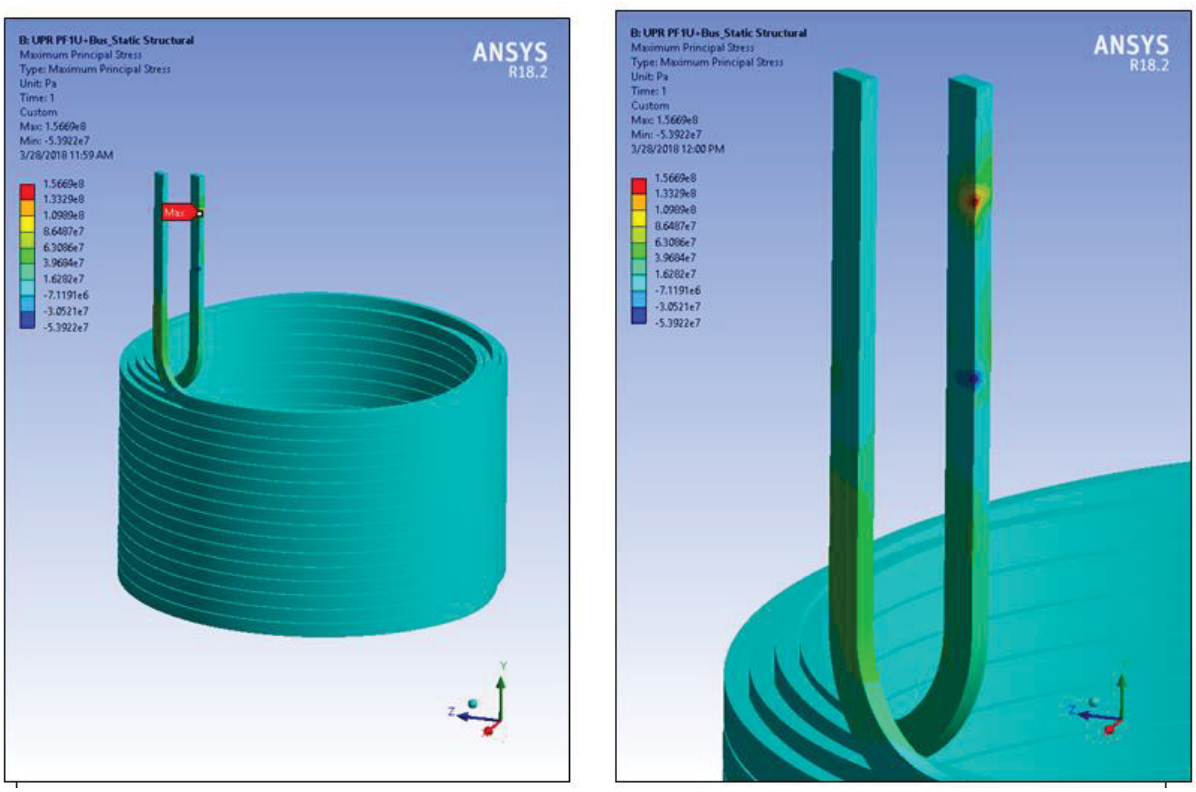

Figure 6.1-8 PF1a Upper –Lead Principal Stress

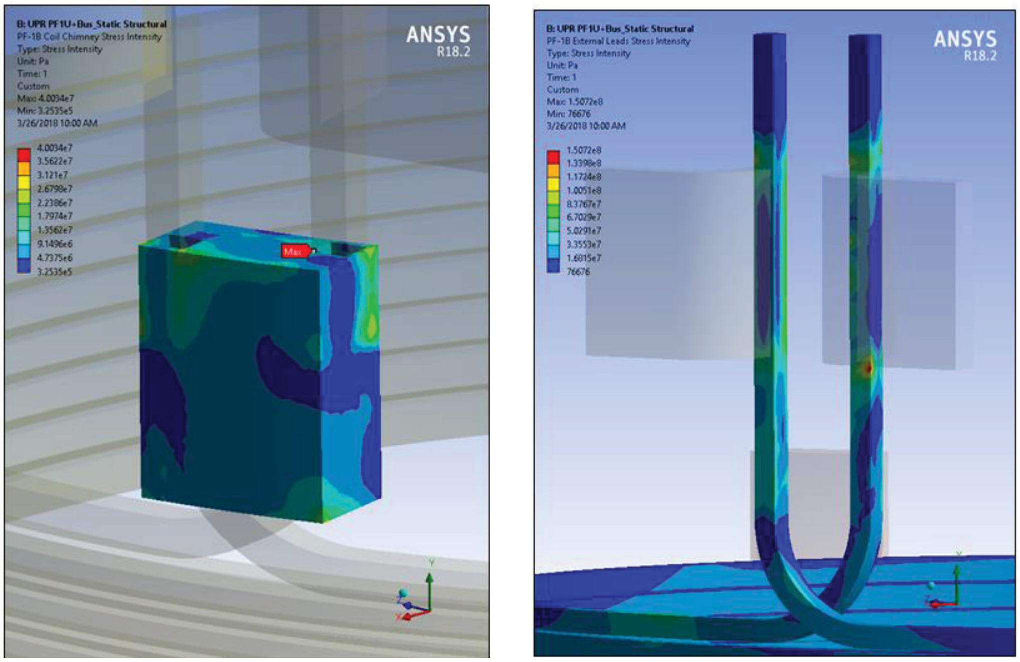

Figure 6.1-9 PF1b Upper – Entrant Block and Lead Stress

The lead stress for PF1bU is 150 MPa, or less than the 160 MPa limit

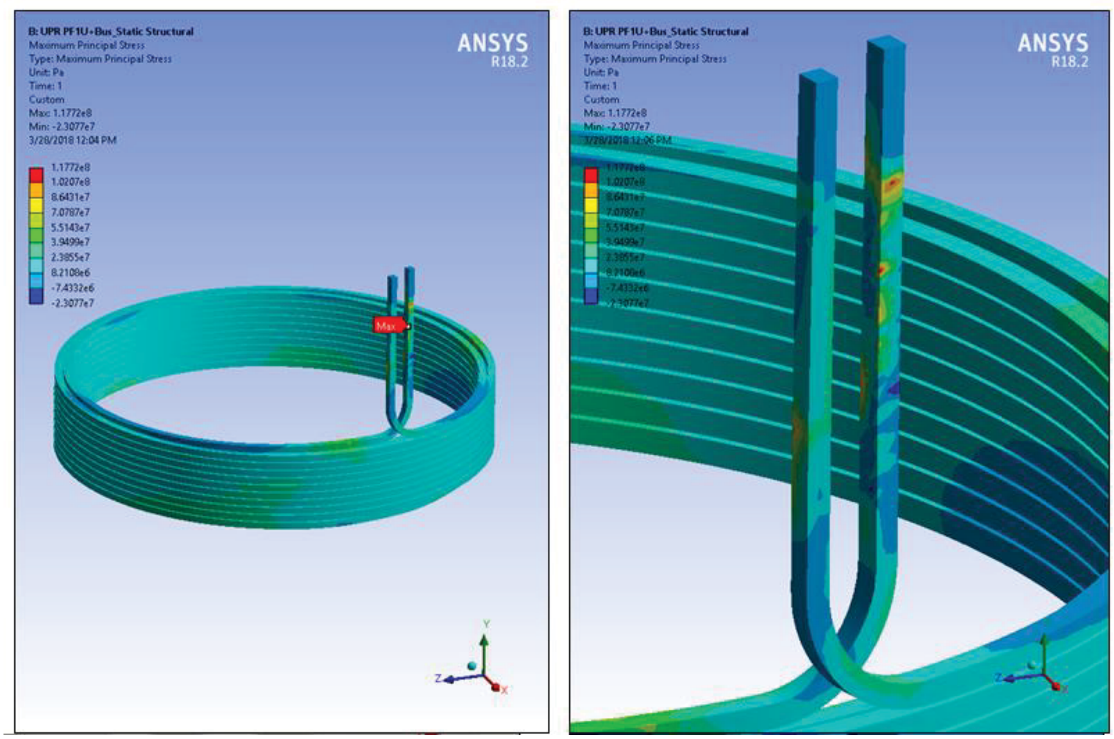

Figure 11 PF1b Upper – Entrant Block and Lead Principal Stress, Reverse TF Current

6.2 PF-1a and -1b Lower Leads and Bus Bars

As in the upper coil analyses the Maxwell loads were transferred to the Workbench model directly.

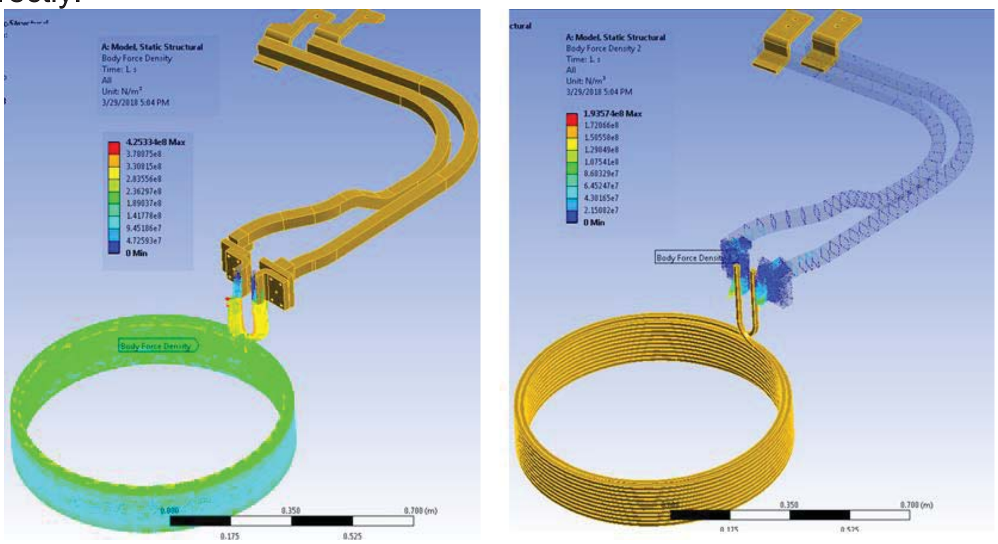

Figure 6.2-1 PF1bL Force Density Plot, At Right Bus Force Density

For the lower coils a thermal case was included for which the PF 1 a coil was set at 60 C,the PF1b coil was set at 90 C and Bus Bars were set at 30C

:xporting Volume Force Density Without Scaling...

Object	Total Force From Maxwell 3D	Total Force Mapped	Ratio
Box2	(0N, 0N, 0N)	(0N, 0N, 0N)	0
JWPF1ALOWERANALYSIS	(996.168N, 98134.7N, 1508.59N)	(1051.63N, 92233N, 1375.22N)	1.06398

Figure 6.2-2 Load Transfer Summation –Maxwell to Workbench

Unlike the upper assembly, the PF-1a and PF-1b lower coil assembly is fixed on the bottom flange. The coil packs can move radially at the lower flange interface but are bonded onto the sling structures at the sling interface. Figure 20 presents the typical displacement from the PF-1b structural model assembly for the EQ #33 reverse field case. The two bus-bars are tied together (bonded contact) at the “L” corner location as shown in Figure 20 to react Lorentz forces on the bus bars and thus minimize its impact to coil leads. The bus bars are fixed at the far end of the coil terminals for the lead analysis.

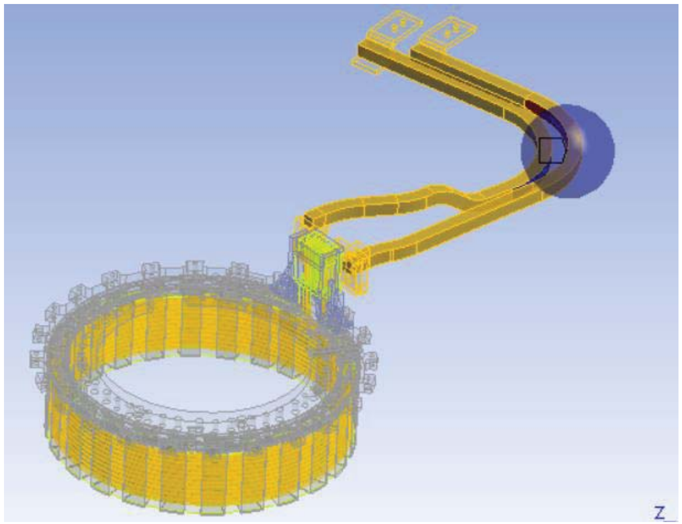

Figure 6.2-2 PF1bL Interconnection Between Bus Implemented with Coupling

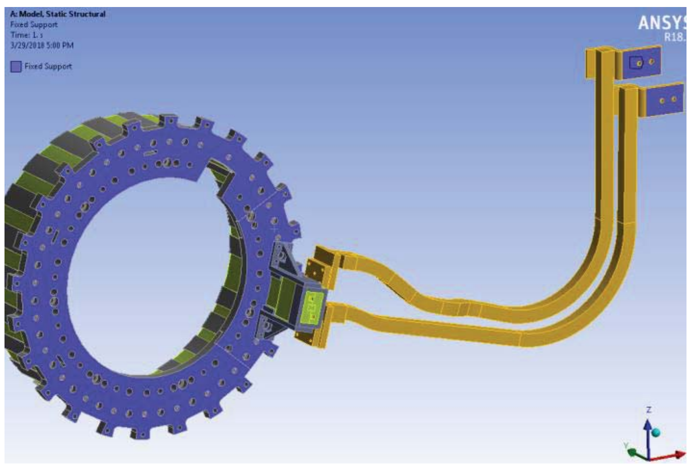

Figure 6.2-3 Constrained Surfaces in the PF1bL Model

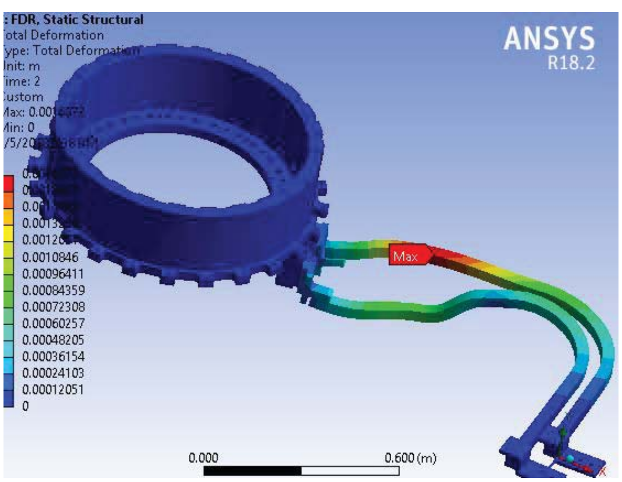

Figure 6.2-4 PF1bL SRSS Displacemt

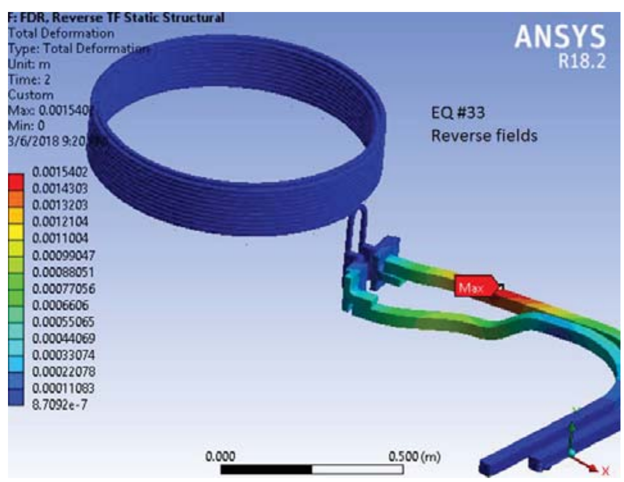

Figure 6.2-4SRSS Displacement Rev TF

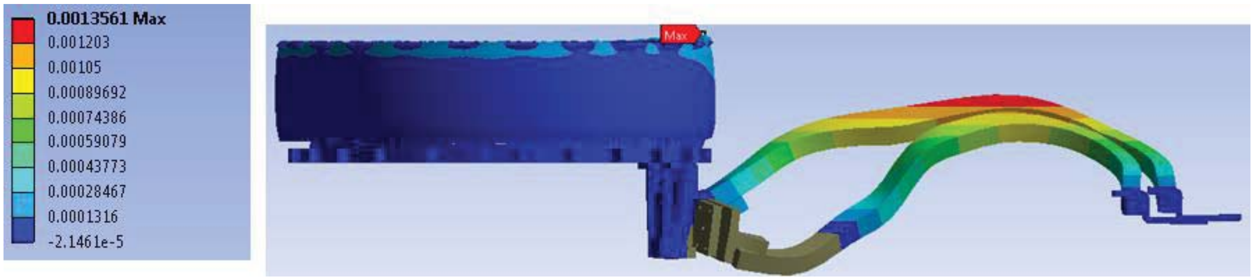

Figure 6.2-5 PF1b Lower – UY Displacement of the coil and bus bar assembly

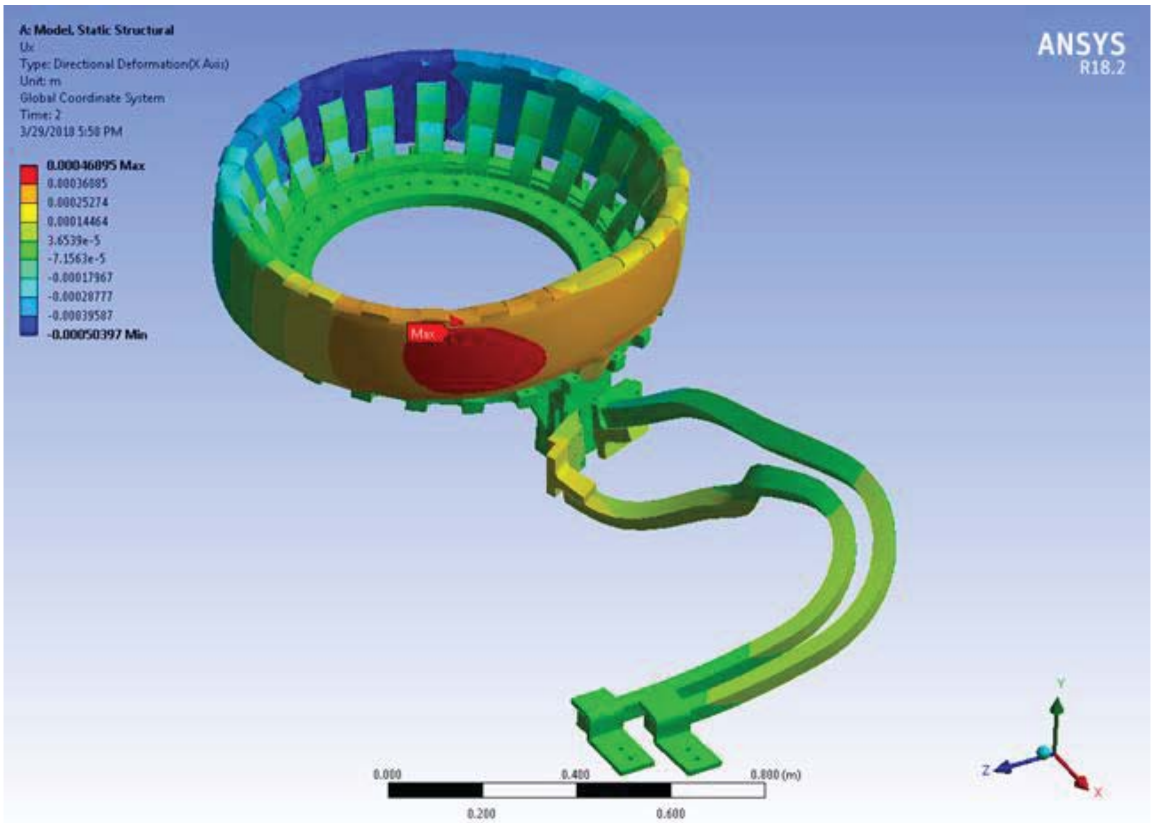

Figure 6.2-6 X Displacement For a Thermal + Lorentz Load Case

Figure 6.2-6 shows the functioning of the sling supports to allow thermal growth of the PF1bl Coil

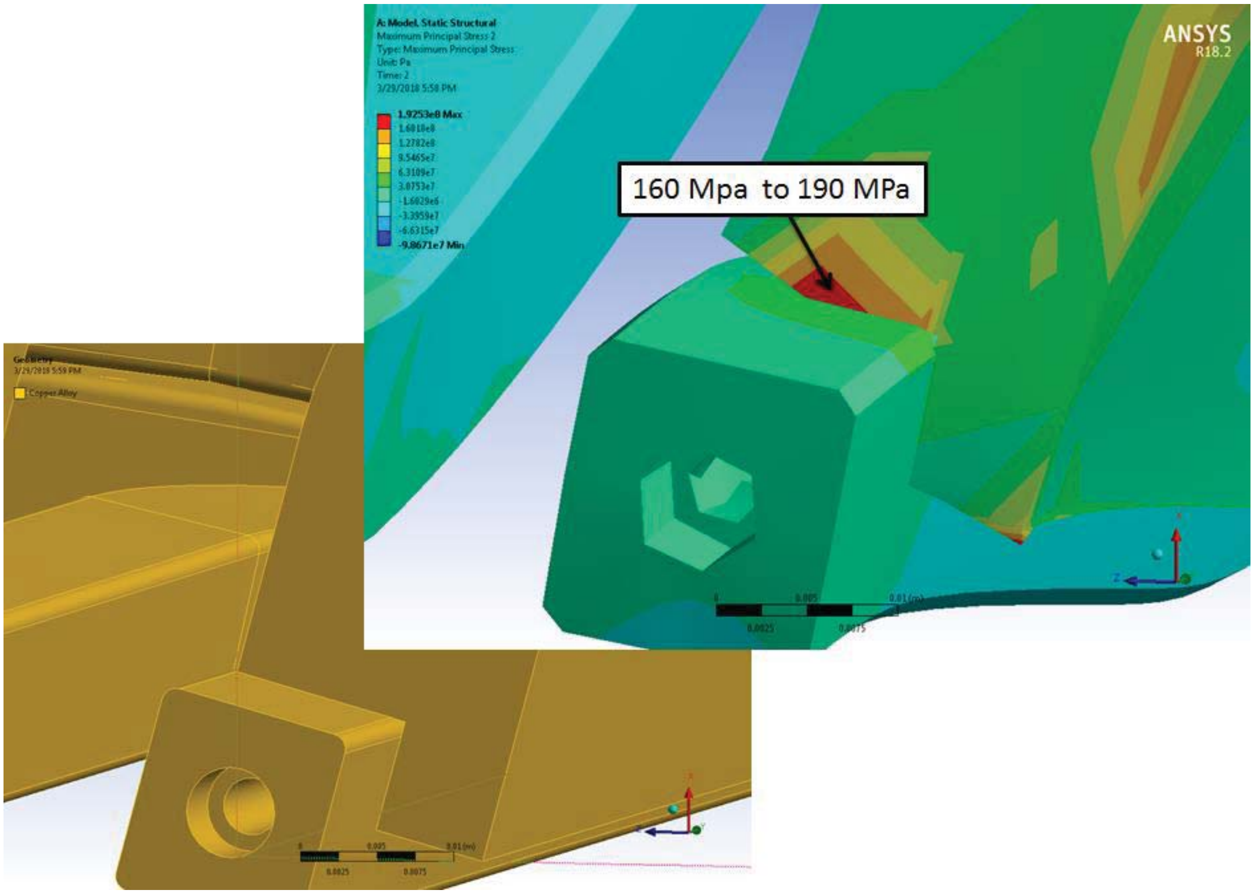

Figure 6.2-7 Peak Stress PF1bL Flag to Conductor joint

Modeling of this intersection is not good. There is a discontinuity in the stress contour, and it does not appear bonded across the width of the joint. This is anothger place where the fillet reinforcement will be important to move the stress away from the coolant hole and reduce the stress concentration.

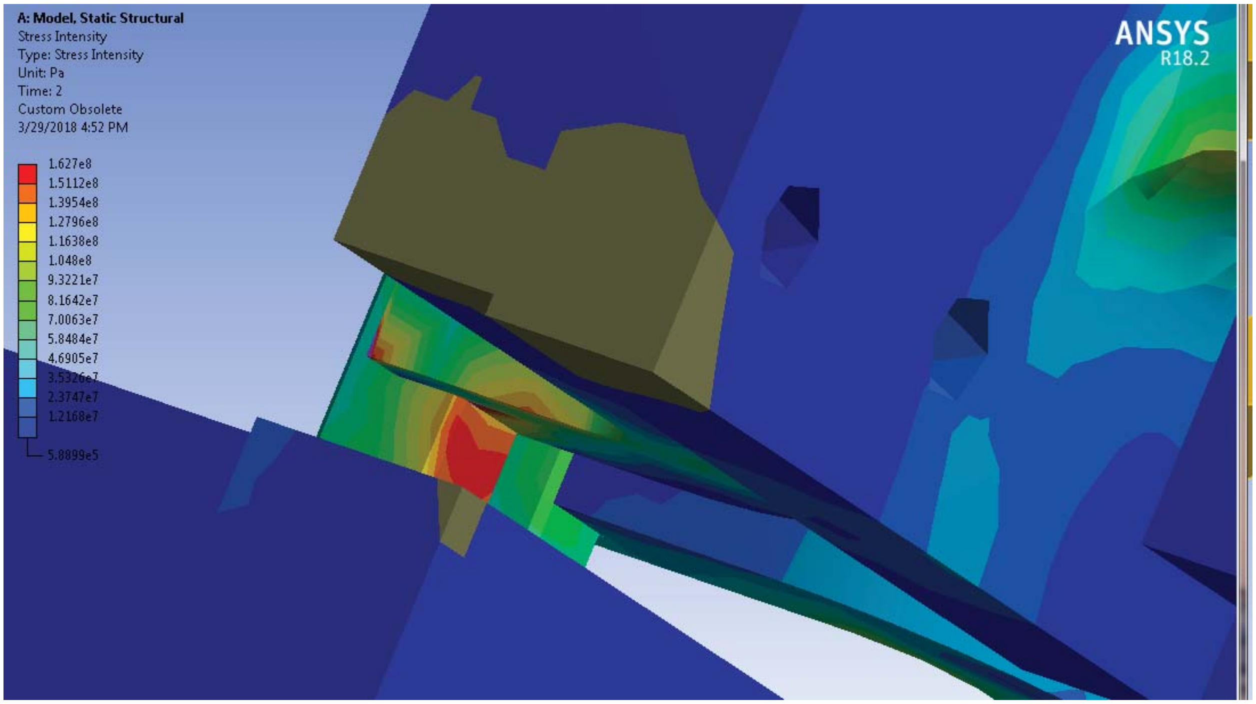

Figure 6.2-13 Peak Stress PF1bL Flag to Conductor joint – 160 MPa

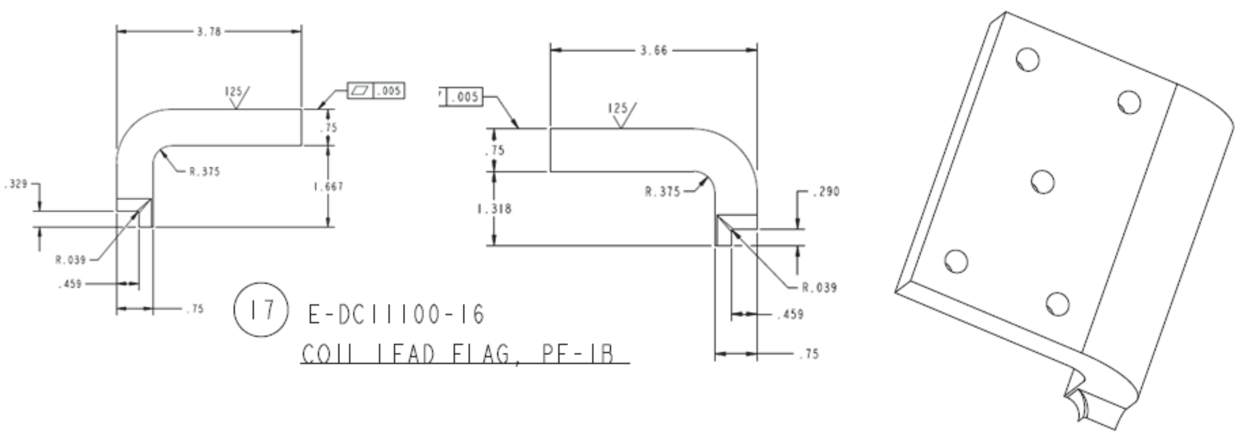

Figure 6.2-14 Drawing Detail of PF1b Flag to Conductor joint

The conductor stress at coil terminals for the case under EM loads (Lorentz forces) is well under control with the new design of the G10 filler blocks and terminal support tower brackets. Figure 21 presents the conductor stress at coil and coil terminals for the worst EQ case Lorentz loads. The peak stress of 87 and 120 MPa for both positive and reverse TF field case (EQ #33) is well within the 160 MPa design limits. Similarly, Figure 22 presents the conductor stress on PF-1a lower terminals for the worst EQ case. The peak stresses of 120 and 145 MPa are also under the 160 MPa fatigue stress limit.

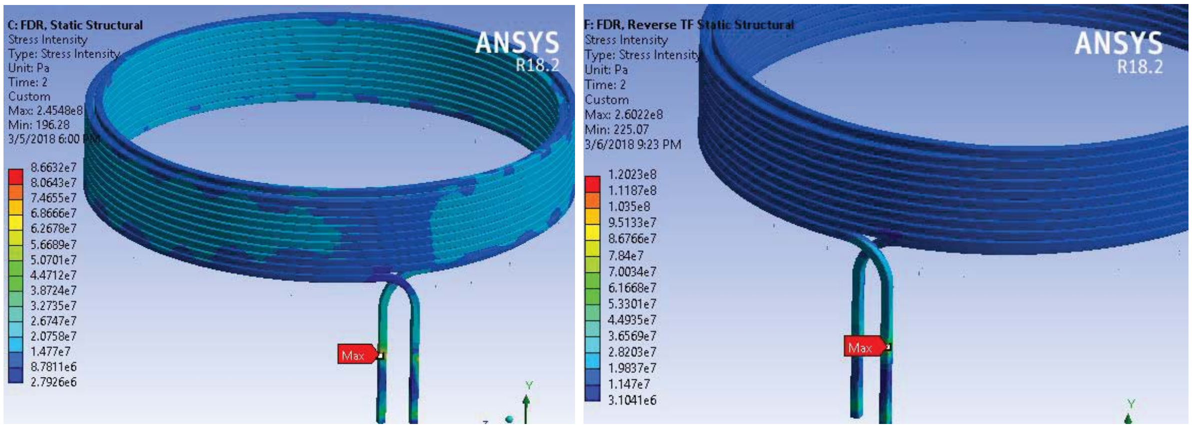

Figure 6.2-5 PF1b Lower – Conductors stress at coil terminals under worst case Lorentz loads

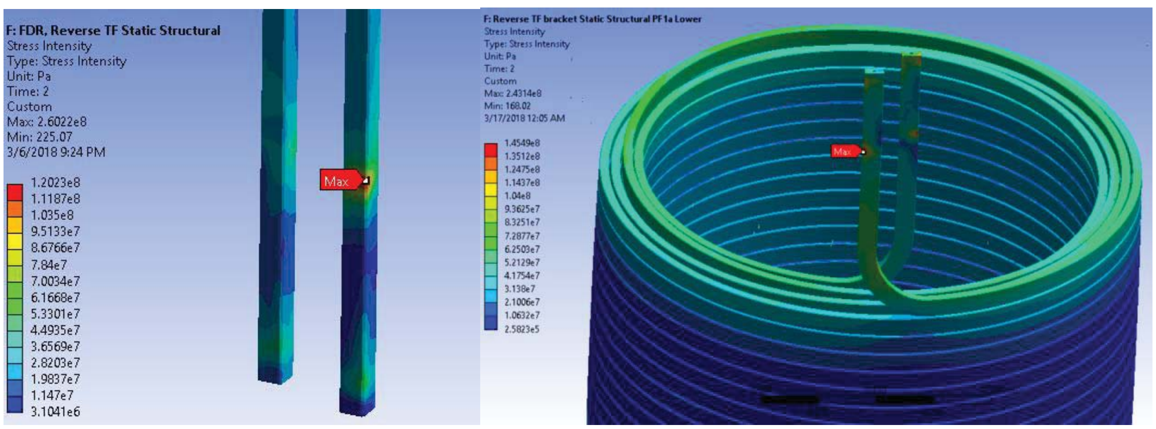

Figure 6.2-6 PF1a - Insulation normal tensile strain during transient cool down

Thermal stresses due to temperature gradient at the terminal regions may contribution noticeably to the total peak stress of the conductors in the lead section. Figures 23 and 24 present the conductor stresses at coil terminals for the worst load case EM loads plus thermal loads (temperature gradients). The coil temperature is prescribed at 60 and 90 C for PF-1a and PF-1c respectively. Figure 25 presents the displacement and stress distribution on the PF-1a lower assembly.

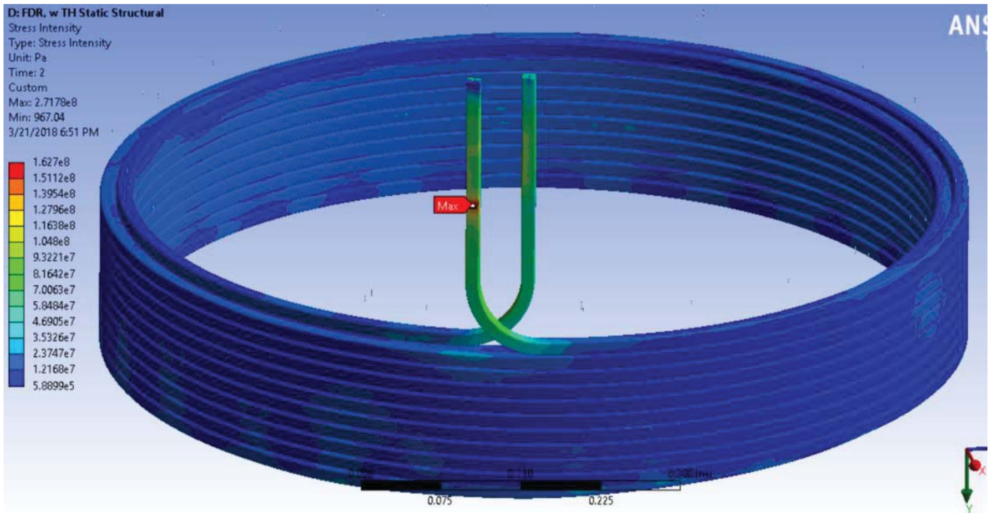

Figure 6.2.7 PF1b – Conductor stress at coil terminals for worst case EM loads and Thermal Loads

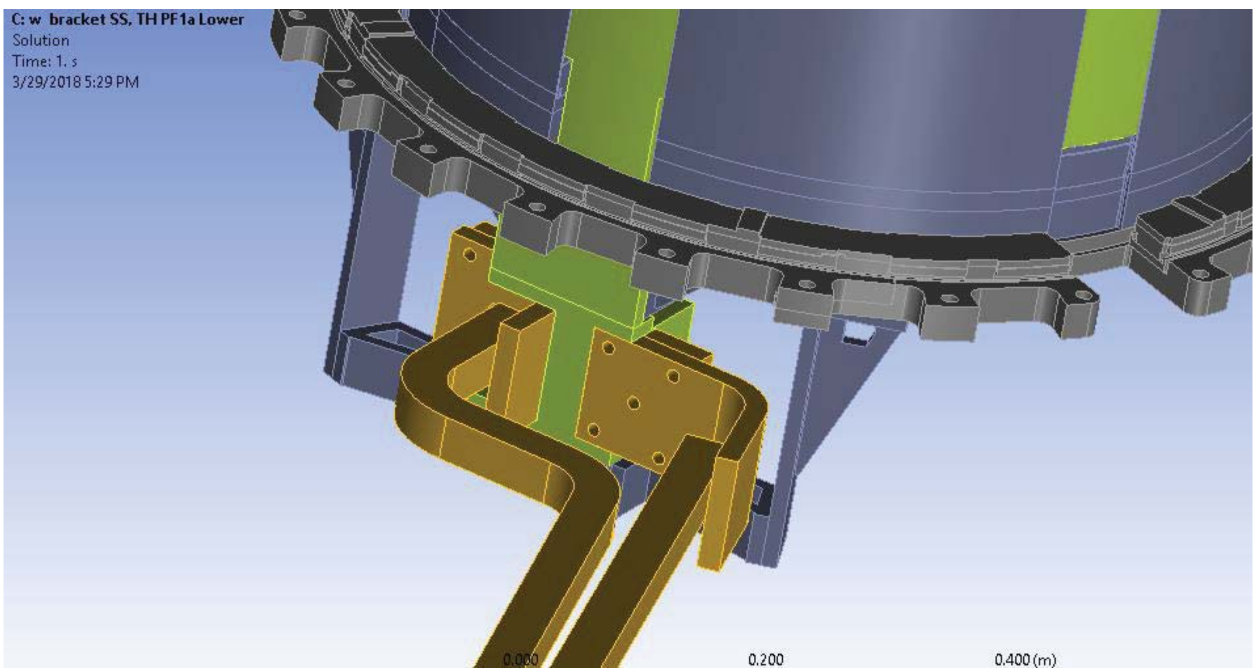

Figure 12 PF1a – Terminal Reinforcements

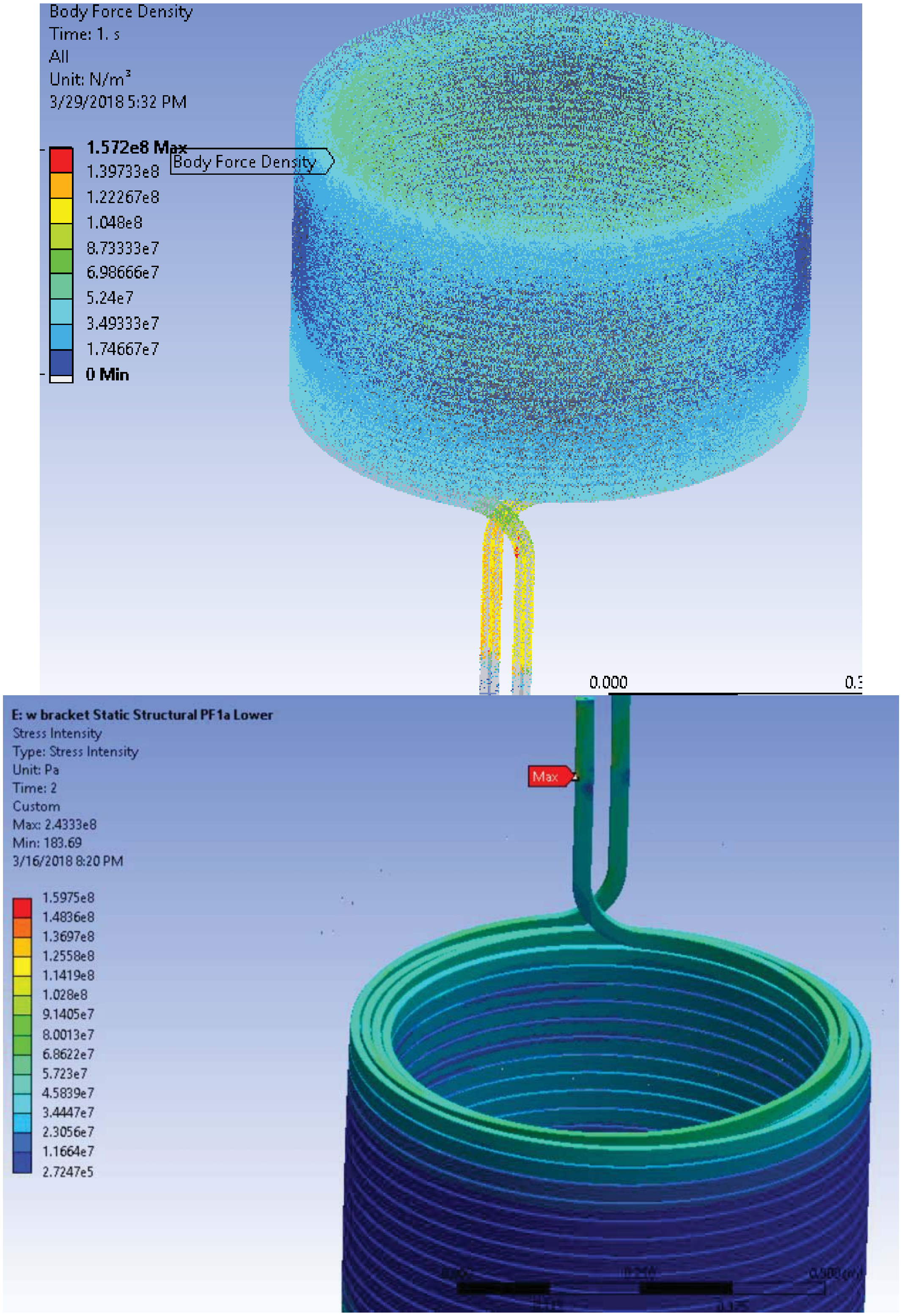

Figure 13 PF1a – Conductor stress at coil terminals for worst case EM loads and Thermal Loads

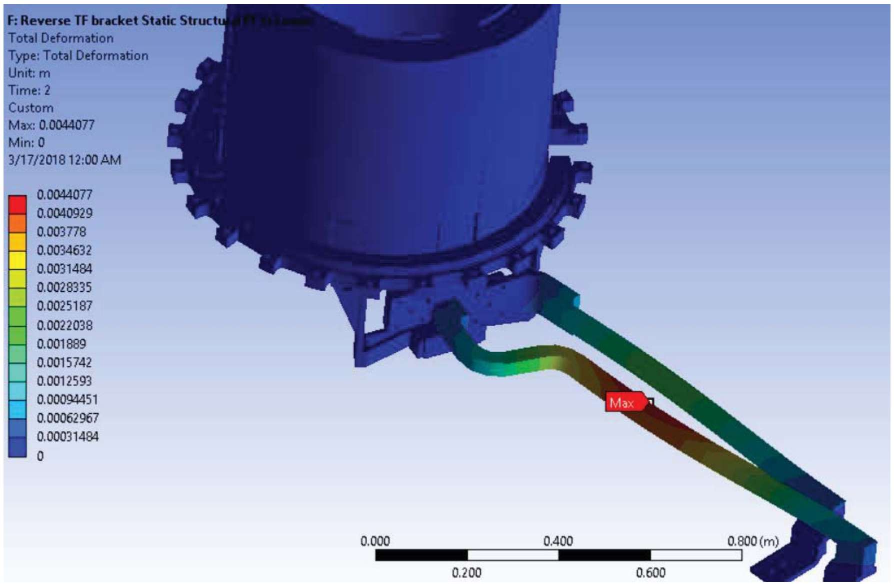

Figure 6.2-10 PF1a Lower – Typical SRSS displacement

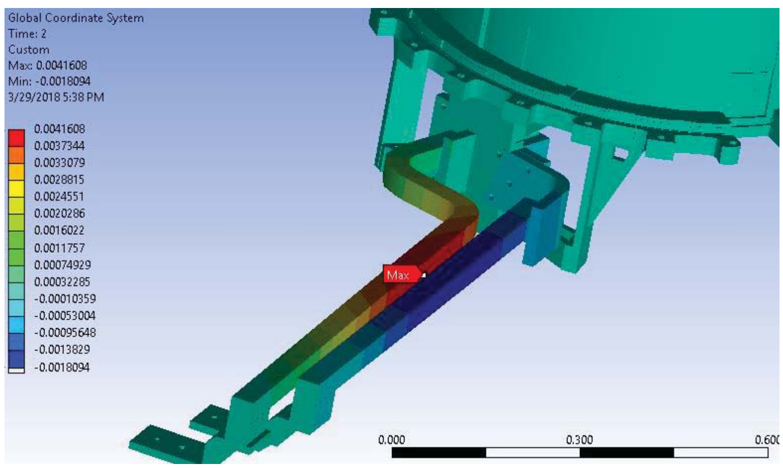

Figure 6.2-11 PF1a Lower – Typical UY displacement

Note that in this analysis the leads crossing the TF field are not interconnected as in leads for other inner PF coils. This is possible because of the much wider reinforcement designed for the Recovery Project than used in the Upgrade design. One flag was bent during the 2016 run and the bent flag that needed to be accommodated in the FCPC tests .

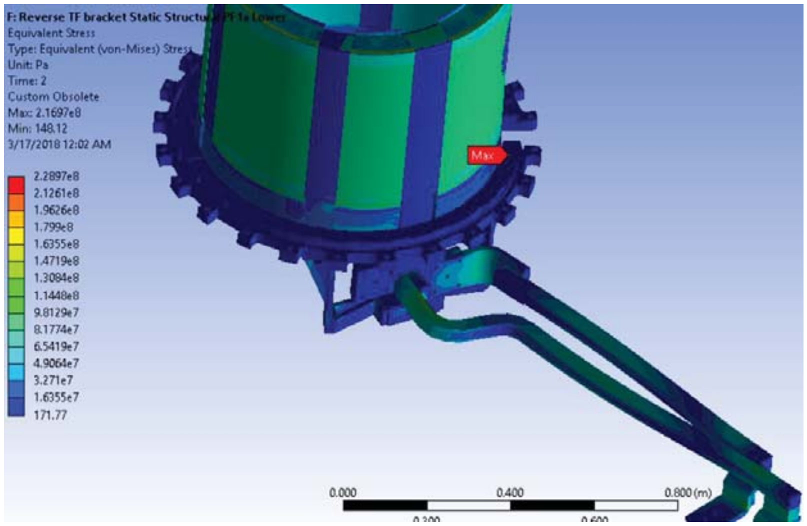

Figure 14PF1a Lower – Typical stress (lower) distribution from PF-1a lower assembly